This is a preprint, the final version is subject to change, of the American Mineralogist (MSA)
Cite as Authors (Year) Title. American Mineralogist, in press.
DOI: https://doi.org/10.2138/am-2019-7028

Revision 1

Gasparite-(La), $La(AsO_4)$, a new mineral from Mn ores of the Ushkatyn-III deposit, Central Kazakhstan and metamorphic rocks of the Wanni glacier, Switzerland

Oleg S. Vereshchagin*[1], Sergey N. Britvin[1,6], Elena N. Perova[1], Aleksey I. Brusnitsyn[1], Yury S. Polekhovsky[1], Vladimir V. Shilovskikh[2], Vladimir N. Bocharov[2], Ate van der Burgt[3], Stéphane Cuchet[4], and Nicolas Meisser[5]

[1]Institute of Earth Sciences, St. Petersburg State University, University Emb. 7/9, 199034 St. Petersburg, Russia

[2]Geomodel Centre, St. Petersburg State University, Uliyanovskaya St. 1, 198504 St. Petersburg, Russia

[3]Geertjesweg 39, NL-6706EB Wageningen, The Netherlands

[4]ch. des Bruyeres 14, CH-1007 Lausanne, Switzerland

[5]Musée cantonal de géologie, Université de Lausanne, Anthropole, 1015 Lausanne, Switzerland

[6]Kola Science Center, Russian Academy of Sciences, Fersman Str. 14, 184209 Apatity, Murmansk Region, Russia

*E-mail: o.vereshchagin@spbu.ru

This is a preprint, the final version is subject to change, of the American Mineralogist (MSA)
Cite as Authors (Year) Title. American Mineralogist, in press.
DOI: https://doi.org/10.2138/am-2019-7028

Abstract

Gasparite-(La), $La(AsO_4)$, is a new mineral (IMA 2018-079) from Mn ores of the Ushkatyn-III deposit, Central Kazakhstan (type locality) and from alpine fissures in metamorphic rocks of the Wanni glacier, Binn Valley, Switzerland (co-type locality). Gasparite-(La) is named for its dominant lanthanide, according to current nomenclature of rare-earth minerals. Occurrence and parageneses in both localities is distinct: minute isometric grains up to 15 μm in size, associated with fridelite, jacobsite, pennantite, manganhumite series minerals (alleghanyite, sonolite), sarkinite, tilasite and retzian-(La) are typically embedded into calcite-rhodochrosite veinlets (Ushkatyn-III deposit), versus elongated crystals up to 2 mm in size in classical alpine fissures in two-mica gneiss without indicative associated minerals (Wanni glacier). Its chemical composition has been studied by EDX and WDX; crystal-chemical formulas of gaspatite-(La) from the Ushkatyn-III deposit (holotype specimen) and Wanni glacier (cotype specimen) are $(La_{0.65}Ce_{0.17}Nd_{0.07}Ca_{0.06}Mn_{0.05}Pr_{0.02})_{1.03}$ $((As_{0.70}V_{0.28}P_{0.02})_{1.01}O_4)$ and $(La_{0.59}Ce_{0.37}Nd_{0.02}Ca_{0.02}Th_{0.01})_{1.00}$ $((As_{0.81}P_{0.16}Si_{0.02}S_{0.02})_{1.00}O_4)$, respectively. In polished sections, crystals are yellow and translucent with bright submetallic luster. Selected reflectance values R_1/R_2 (λ, nm) for the holotype specimen in air are: 11.19/9.05 (400), 11.45/9.44 (500), 10.85/8.81 (600), 11.23/9.08 (700). Features of the crystal structure of gasparite-(La) were studied by means of EBSD (holotype specimen), XRD and SREF (cotype specimen). Gasparite-(La) has a monoclinic structure with the space group $P2_1/n$. Our studies revealed that gasparite-(La) from the Ushkatyn-III deposit and Wanni glacier have different origins. La/Ce and As/P/V ratios in gasparite-(La) could be used as an indicator of formation conditions.

Keywords: gasparite-(La), new mineral, arsenate, REE, Mn ores, monazite-type structure, Ushkatyn-III, Kazakhstan, Wanni glacier, Binn Valley, Switzerland

Introduction

In the course of this study, we described a new rare-earth element (REE) arsenate-gasparite-(La) ($La(AsO_4)$, IMA 2018-079) from the Ushkatyn-III deposit, Central Kazakhstan and the Wanni glacier, Binn Valley, Switzerland. Gasparite-(La) is named for the dominant lanthanide according to current nomenclature of REE minerals (Bayliss and Levinson 1988).

The type locality of gasparite-(La) is the Ushkatyn-III deposit, Central Kazakhstan. Minute isometric grains of gasparite-(La) up to 15 μm in size were discovered in samples from the Ushkatyn-III deposit collected during field work in 2017. The holotype specimen of gasparite-(La) was deposited at the Mineralogical Museum of St. Petersburg State University, St. Petersburg, Russia, catalogue number 19692.

The co-type locality of gasparite-(La) is the Wanni glacier, Binn Valley, Valais, Switzerland. Elongated crystals of gasparite-(La) up to 2 mm in size were discovered in autumn 2005 and visually classified as "monazite." Because of their unusual appearance, the material was subjected to further analyses, and recognized as likely identical to the gasparite-(La) later discovered in the Ushkatyn-III deposit. The cotype specimen from Wanni glacier is preserved in Musée Cantonal de Géologie in Lausanne under catalogue number MGL 093518.

The use of crystals from different localities allowed us to describe the whole range of physical and chemical properties of gasparite-(La), investigate its crystal chemistry and identify some features characteristic of different genetic types of deposits.

REE-arsenates are among rare minerals: CNMNC IMA has approved only 14 mineral species to date. Most of them representative of Ce-dominant species and only 3 La-dominant minerals have been discovered (Dunn et al. 1984; Mills et al. 2010; Modresky 1983).

Despite the limited number of approved mineral species, REE-arsenates are widely distributed in distinct mineral assemblages on numerous localities. Mineralogical information

about arsenates (both discovered and crystal-chemical characteristics) provide a key to understanding the occurrence and subsequent evolution of many localities (e.g., Campbell and Nordstrom, 2014; Majzlan et al. 2014; Wu et al. 2018; Yang et al. 2018).

REE-arsenates have been reported from several postmagmatic and metasedimentary rocks, whose mineral composition was strongly influenced by late hydrothermal fluids (metasomatic replacement). In the Slovak rhyolites (Ondrejka et al. 2007), primary monazite-(Ce) and xenotime-(Y) were transformed into secondary gasparite-(Ce) and chernovite-(Y), respectively. In case of the granite cupola at Zinnwald (Germany) or Cínovec (Czech Republic), As-rich hydrothermal fluids dissolved and severely altered primary magmatic REE–Y–Th–U–Zr mineralization and gave rise to the formation of *REE*-arsenates: arsenoflorencite-(Ce), chernovite-(Y), and hydrous xenotime(Y)-chernovite-(Y) solid solutions (Förster et al. 2011). In the Hora Svaté Kateřiny granite (Czech Republic), reaction with oxidizing As-bearing fluids caused the decomposition of xenotime-(Y), and led to the precipitation of chernovite-(Y) and the incorporation of As into altered zircon and thorite (Breiter et al. 2009). Migrating As-bearing solutions are also believed to have formed the remarkable, classical assemblage of numerous arsenates and arsenites in the Wanni glacier/Mt. Cervandone area at the frontier between the Binn Valley (Switzerland) and Alpe Devero (Italy) (Graeser and Roggiani 1976, Guastoni et al. 2006; Hofmann and Knill 1996). Besides indirect evidence of the presence of multiple REE-arsenates in close association, several minerals show direct evidence of originating from such fluids: gasparite-(Ce) was found as a reaction rim around synchisite-(Ce) (Graeser and Schwander 1987); deveroite-(Ce) was found as a dissolution product of cervandonite-(Ce) (Guastoni et al. 2013); agardite-(Y) (Gatta et al. 2018), rhabdophane-(La) and uranyl arsenates on cafarsite (Appiani et al. 2017).

Manganese rocks of different genesis are often enriched in arsenic, reaching

concentrations several times higher than the mean values for both sedimentary rocks and for the upper part of the continental crust as a whole (Li and Schoonmaker 2003; Maynard 2003). More than half of all discovered Mn-arsenates were found in the famous Mn deposits in Franklin/Sterling Hill, USA; Långban, Sweden and Moss Mine, Sweden.

Both Långban, Sweden and Franklin/Sterling Hill, New Jersey, USA are represented by strongly metamorphosed Precambrian rocks of sedimentary origin (Frondel and Baum 1974; Holtstam and Langhof 1999; Lundström 1999). According to Frondel and Baum (1974), the only primary As-bearing ore minerals in Franklin/Sterling Hill are löllingite, arsenopyrite and the calcium arsenate svabite. In both cases (Långban and Franklin / Sterling Hill), the greatest mineralogical diversity is found among the minerals in veins and fissures.

A limited number of small Fe–Mn–(Ba,V,As,Sb,Be,W,REE) deposits, containing both arsenates and REE-arsenates, have been found and studied in the Swiss, Italian and Austrian Alps (Abrecht 1990; Brugger and Giere 1999; Brugger and Meisser 2006; Cabella et al. 1999). These occurrences are thought to represent syngenetic exhalative Fe-Mn accumulations (Majzlan et al. 2014) metamorphosed during the Alpine orogeny (Abrecht 1990; Brugger and Meisser 2006). Brugger and Meisser (2006) argued that the chemical composition of the rocks reflects the pre-metamorphic state. Cabella et al. (1999) reported that the abundance of arsenates reduces sharply as a function of proximity to the Fe-Mn ores. The same genetic conclusion was made for Mn-rich metamorphic rocks in the Hoskins manganese mine, New South Wales, Australia (Ashley 1989).

Gasparite-(Ce) is, although generally rare, the most widely distributed REE-arsenate. The type locality for gasparite-(Ce), and several other REE-arsenates and arsenites, is Mt. Cervandone, a summit on the frontier of Italy (Cervandone, Val Devero) and Switzerland (Wanni glacier, Binntal), where it occurs in metasedimentary rocks (Graeser and Schwander 1987). Besides that, gasparite-(Ce) was found as an accessory mineral in the Black Range Tin

120 District, New Mexico, USA (Foord et al. 1991); Tisovec-Rejkovo, Slovakia (Ondrejka et al.
121 2007); Beryllium Virgin Claim, New Mexico, USA (Anthony et al. 2000); Chudnoe and
122 Nesterovskoe occurrences, Maldynyrd Range, Prepolar Ural, Russia (Moralev et al. 2005);
123 Kesebol deposit, Sweden (Kolitsch and Holtstam 2004; Kolitsch et al. 2004); Grubependity
124 Lake cirque, Maldynyrd Range, Prepolar Ural, Russia (Mills et al. 2010); Artana, Carrara,
125 Apuane Alps, Italy (Mancini 2000); Tanatz Alp, Switzerland (Roth and Meisser 2013) and
126 Ponte dei Gonazzi, the Maritime Alps, Italy (Cabella et al. 1999).

127 In most cases, lanthanum is present in gasparite in subordinate amounts (< 15 wt%
128 La_2O_3). However, La-dominant grains of gasparite were found in Mn-enriched
129 metamorphosed rocks from the Ponte dei Gonazzi, the Maritime Alps, Italy (up to 45 wt%
130 La_2O_3; Cabella et al. 1999) and in A-type rhyolite from Western Carpathians, Slovakia (up to
131 26 wt% La_2O_3; Ondrejka et al. 2007). Particle size was insufficient to allow for the
132 investigation of the properties of La-dominant gasparite, and therefore these studies did not
133 describe their findings as a new mineral phase.

134 ## Occurrence

135 **Ushkatyn-III deposit, Central Kazakhstan**

136 The Ushkatyn-III deposit (48°16'06"N, 70°10'43"E) is located in Central Kazakhstan
137 300 km southwest of the city of Karaganda and 20 km to the northeast of the village
138 Zhayrem. The deposit was discovered in 1962. Manganese ore mining started in 1982 and
139 continues to date. Beginning from 2015, barite-lead ores started to be mined. As of 2015,
140 manganese ore reserves amounted to 102 million tons, with an average Mn content of 24 wt%
141 and Fe 3.5 wt%, and barite-lead ore reserves of 42 million tons, with an average Pb-2.6 wt%,
142 $BaSO_4$-19 wt% (JSC "Zhayremsky ore mining and processing enterprise," 2015).

143 The geological structure of the deposit was considered in the works of Kayupova
144 (1974), Buzmakov et al. (1975), Mitryaeva (1979), Rozhnov (1982) and Skripchenko (1980,

1989). The Ushkatyn-III deposit is located in the western part of the Zhailinsky graben-syncline. This large riftogenic structure originated in the Late Devonian during the destruction of the epi-Caledonian Central-Kazakhstan continental block. The clay-siliceous-carbonate rocks of the Famennian stage of the Upper Devonian are ore-bearing. In the eastern part of the deposit, they are represented by reefogenic limestones containing a stratiform barite-lead mineralization. In the western part of the deposit, these rocks are replaced by detrital and nodular-layered siliceous limestones containing layers of manganese ores. Altogether, there are fourteen ore layers, each of which has a well-marked, rhythmically-stratified structure with alternating layers of manganese ore and limestones. The thickness of individual rhythms range from 15 cm up to 1 m, and the total thickness of ore layers varies from 5 to 25 m. A series of adjacent layers is grouped into a large pack, traced over a strike of more than 1.5 km, a drop of 760 m and a thickness of 50–150 m. Volcanic rocks are present on the deposit but in volumetric inferior amount (no more than 10% of the hole volume of the ore-bearing strata).

Manganese ores are fine-grained rocks (average size of mineral grains 10–30 μm) with layered and lenticular-banded textures. Altogether, more than 60 minerals have been identified in manganese ores of the Ushkatyn-III deposit by optical, electron microscopy, X-ray powder and microprobe analysis (Brusnitsyn et al. 2017, 2018; Kayupova 1974). The main minerals are braunite, hausmannite, quartz, calcite, rhodochrosite, tephroite, friedelite and minerals of manganhumite series (sonolite, alleghanyite). The most characteristic secondary minerals are hematite, jacobsite, rhodonite, caryopilite, pennantite, manganese clinochlore, albite and barite. Among the most interesting accessory minerals are cinnabar, pyrobelonite, cerianite-(Ce), fluorite and several REE and arsenate minerals: sarkinite, svabite, tilasite, retzian group minerals.

Manganese ores could be divided into two types: 1) braunite: braunite + calcite +

quartz ± albite, and 2) hausmannite: hausmannite + calcite + rhodochrosite ± tephroite (sonolite, alleghanyite) ± friedelite (caryopilite). These types of ores can form separate layers, and can be combined within a single layer. In the latter case, the mineral composition of ores change as a result of substitution of braunite for hausmannite/associated silicates/rhodochrosite.

The first arsenates in the Ushkatyn-III deposit were discovered in the early 70s (Kayupova 1974). However, due to the lack of technical equipment, only relatively big grains of minerals (sarkinite, tilasite and brandtite) could be identified.

Gasparite-(La) was found in hausmannite ores, associated with other arsenates. The mineral was found in microveins cutting layers of hausmannite, calcite, rhodochrosite. Gasparite-(La) is associated with fridelite, jacobsite, pennantite, manganhumite series minerals (alleghanyite, sonolite), sarkinite, tilasite and retzian-(La). The microveins containing gasparite-(La) range in size from microns to 1–5 mm in thickness and to 1–3 cm in length. Gasparite-(La) forms grains of 2–25 μm in size, as well as aggregates with other arsenates of irregular shape up to 50 μm and was found in association with retzian-(La) and alleghanyite (Figure 1a).

Wanni glacier, Binn Valley, Valais, Switzerland

The Wanni glacier, located in the Binn Valley, Valais (Wallis), Switzerland, represents the Swiss side of the Scherbadung or Pizzo Cervandone, of which the Italian side is located in Alpe Devero, Piemonte, Italy. Its mineral assemblage extends to both sides of this mountain and is the type locality of seven REE-arsenates and REE-arsenites (Armbruster et al. 1988; Demartin et al. 1994; Graeser 1966; Graeser and Schwander 1987; Graeser et al. 1994; Guastoni et al. 2006, 2013) and its geology has been summarized in Streckeisen et al. (1974), Steck (1987), Klemm et al. (2004), Hettman et al. (2014) and Bergomi et al. (2017). The REE-As mineralization is hosted in two-mica gneisses of the Monte Leone nappe and

195 extends multiple km westward to the Gischi glacier (Graeser and Roggiani 1967),
196 Chummibort (Cuchet et al. 2005) and Mättital (Krzemnicki 1992, 1997) and eastwards to the
197 Lercheltini area. According to Krezemnicki and Reusser (1998), several Pre-alpine ore
198 concentrations within this nappe were locally re-mobilized during Alpine metamorphism,
199 thus generating some unique hydrothermal mineralization.

200 The sample with gasparite-(La) was found in rocks of the Monte Leone nappe
201 (46°19′20,N, 8°12′48E; Hettman et al. 2014; Klemm et al. 2004). The Monte Leone nappe
202 includes fine-grained banded orthogneisses and minor coarse-grained augen gneiss
203 interlayered with paragneisses, hornblende gneisses and amphibolites and shows a
204 penetrative amphibolite-facies metamorphic overprint of Alpine age (Bergomi et al. 2017;
205 Maxelon and Mancktelow 2005).

206 The specimen with gasparite-(La) was extracted from a small, classical Alpine fissure.
207 The stratum containing the fissure with gasparite-(La) is a fine-layered, two-mica gneiss and
208 is located outside the main Cu-As-F-mineralization which has cafarsite as the dominating As-
209 containing mineral (Cuchet et al. 2014, 2016). Based on our observation, the As-enrichment
210 is not very dense in this sublayer. Within the occurrence of *REE*-arsenates (chernovite-(Y),
211 gasparite-(Ce)) is increased, whereas arsenites (cafarsite and asbecasite) are a diminished
212 gasparite form of microcrystalline pseudomorphoses to synchysite-(Ce).

213 The specimen with gasparite-(La) (containing three elongated crystals) was located on
214 one side of the cavity; the remainder was empty, apart from minerals that belong to the
215 classical fissure parageneses: minor titanite, quartz, feldspar and albite. Crystals of gasparite-
216 (La) are prismatic of a size up to 2 mm (Figure 1b). An interesting feature of the studied
217 crystals is that their prism appears non-translucent (as if fractured) and yellow, whereas the
218 summit faces are perfectly, gemmy translucent and more orange.

219 ## Elemental composition

Elemental compositions of rock-forming minerals were studied on the carbon-coated polished sections by means of a Hitachi S-3400N scanning electron microscope equipped with an Oxford X-Max 20 energy dispersive x-ray spectrometer (EDX). EDX spectra were obtained under the following conditions: 20 kV accelerating voltage and 2 nA beam current with an acquisition time of 30 s per spectrum.

Elemental analyses for gasparite-(La) were obtained using an Inca Wave 500 wavelength dispersive x-ray (WDX) spectrometer also equipped on the microscope mentioned above. WDX spectra collection conditions were: 20 kV, 10 nA, beam diameter 5 μm, 30 sec peak and 30 sec background collection per element, XPP matrix correction. Fe metal, Mn metal, V metal, InP, InAs, wollastonite, Th-, Y-, La-, Ce -, Nd- and Sm-bearing glass standard samples (MAC-standards) were used for spectrometer calibration.

Preliminary EDX analyses showed that gasparite-(La) from the Ushkatyn-III deposit had almost no chemical zoning or stable element ratios; all analyzed grains showed La>Ce>Nd and As>V>P. In the case of gasparite from the Ushkatyn-III deposit, Central Kazakhstan five analyses (WDX) from three different grains were performed in one carbon-coated polished section (Table 1). The empirical formula of gasparite-(La) from the Ushkatyn-III deposit based on 4 oxygen is $(La_{0.65}Ce_{0.17}Nd_{0.07}Ca_{0.06}Mn_{0.05}Pr_{0.02})_{1.03}((As_{0.70}V_{0.28}P_{0.02})_{1.01}O_4)$.

One elongated crystal of gasparite from Wanni glacier was studied by EDX and WDX analyses. EDX analysis showed that the crystal had chemical zoning: its La/Ce/Nd ratio varied significantly, whereas As/P ratio was stable (Figure 2). The optically more translucent summit of the crystal was La-dominant, while the prismatic part of the crystal was Ce-dominant; and thus, represents gasparite-(Ce). We performed five WDX analyses from the summit of the crystal and the overall empirical formula of gasparite-(La) from the Wanni glacier based on 4 oxygen is $(La_{0.59}Ce_{0.37}Nd_{0.02}Ca_{0.02}Th_{0.01})_{1.00}((As_{0.81}P_{0.16}Si_{0.02}S_{0.02})_{1.00}O_4)$.

The simplified formula of gasparite-(La) from both the Ushkatyn-III deposit as the Wanni glacier was $La(AsO_4)$.

Gasparite-(La) belongs to the monazite group, which contain seven monoclinic phosphate and arsenate minerals (Table 2). It is a La-dominant analog of gasparite-(Ce) (Graeser and Schwander 1987) and arsenate-dominant analog of monazite-(La). According to the Nickel-Strunz Classification, gasparite-(La) belongs to 8.AD (8: phosphates, arsenates, vanadates, A: phosphates, etc. without additional anions, without H_2O, D: with only large cations).

Physical properties and optical data

Gasparite-(La) crystals are yellow and translucent with bright submetallic luster. The Vickers Hardness Number (VHN) measured on gasparite-(La) from the Wanni glacier was 325 with a range 308–340 kg mm^{-2} (load 20 g) by means of HMV-2T (Shimadzu). This data is in a good agreement with data on gasparite-(Ce) (VHN=327 kg mm^{-2}; Graeser and Schwander 1987). Mohs hardness could not be determined because of the tiny size of the crystals. The Mohs hardness calculated from the VHN value was approximately 4½.

As gasparite-(La) from the Ushkatyn-III deposit had no chemical zoning, one of its grains was chosen for optical study. In polished sections, gasparite-(La) from the Ushkatyn-III deposit looked dark gray in reflected light. The mineral was slightly anisotropic with Δ R_{589} = 2.04%. The reflectivity of gasparite-(La) in air (Table 3) was measured against a SiC standard (Reflexions standard - 474251, No. 545) using MSF-21 spectrophotometer with a monochromator slit of 0.4 mm and a 100 μm zone diameter. The measurement parameters were as follows: lens magnification 21x, aperture 0.4 and $\Delta\lambda$=10 nm, SiC. The reflectivity spectrum is shown in Figure 3.

Raman spectra

Gasparite-(La) crystals from both localities were used for Raman studies. Raman spectra (Figure 4) were recorded with a Horiba Jobin-Yvon LabRAM HR800 spectrometer

equipped with an Olympus microscope. The microscope comprised 50x and 100x objectives. Raman spectra were excited by an Ar ion laser at a wavelength of 514 nm and a maximum power of 50 mW. The spectra were obtained in the range of 100-4000 cm^{-1} at a resolution of 2 cm^{-1} at room temperature. To improve the signal-to-noise ratio, the number of acquisitions was set to 20. The spectra were processed using licensed Labspec and Origin software . Band fitting was done using a Lorentz function with the minimum number of component bands used for the fitting process (Table 4).

Raman spectra of gasparite-(La) from both the Ushkatyn-III deposit and the Wanni glacier were very close to synthetic $La(AsO_4)$ (Fig. 4, Table 4). Bands in the region from 4000 to 1100 cm^{-1} were not registered, which means that gasparite-(La) contained no $(OH)^-$ groups. Bands assigned to stretching vibrations v_1 and v_3 of arsenate ion are observed in the region 900-800 cm^{-1}. There were bending vibrations v_2 and v_4 of arsenate ion in the region of 500–350 cm^{-1}. The lattice vibrations were located below 320 cm^{-1}. The main differences of Raman spectra of the minerals in comparison with the pure synthetic phase were associated with impurities of $(VO_4)^{3-}$ (Ushkatyn-III) and $(PO_4)^{3-}$ (Wanni glacier). Vibrations $v_1(PO_4)$ was about 960 cm^{-1}, $v_1(VO_4)$ – near 840 cm^{-1} (Song et al. 2018; Solecka et al. 2018). In the region of the v_4 band the main differences connected with the overlapping of bands related to $(AsO_4)^{3-}$, $(PO_4)^{3-}$ and $(VO_4)^{3-}$. Raman spectra pointed out predominance of La+Ce in the mineral composition of $v_1(AsO_4)$ of 861–863 cm^{-1}. The Raman spectrum of $Ho(AsO_4)$ $v_1(AsO_4)$ was about 895 cm^{-1} (Barros et al., 2009). Impurity tetrahedral cations (P,V) did not influence the $v_1(AsO_4)$ band shift.

Crystallography

Because gasparite-(La) from the Ushkatyn-III deposit occurs as microscopic grains up to 15 μm in size (Fig. 2) it was not possible to determine its crystal structure with a single crystal X-Ray diffraction. All diffraction data were obtained by electron backscatter

diffraction (EBSD). In the case of gasparite-(La) from the Wanni glacier, we managed to isolate the La-enriched zone of the elongated crystal and refine its crystal structure using single crystal X-Ray diffraction. The same crystal fragment was used for powder X-ray diffraction studies.

Powder X-ray diffraction (XRD).

The powder XRD pattern for gasparite-(La) from the Wanni glacier was recorded in Debye–Scherrer geometry by means of a Rigaku R-AXIS Rapid II diffractometer equipped with a curved (cylindrical) imaging plate detector (r=127.4 mm). CoKα radiation (λ=1.79021 Å) was generated by a rotating anode (40 kV, 15 μA) with microfocus tube optics; exposure time was set to 15 min. The data were processed using the osc2xrd program (Britvin et al. 2017) and Stoe WinXPOW software (Stoe and Cie 2006). XRD data for gasparite-(La) from the Wanni glacier is presented in Table 5 and was similar to synthetic $La(AsO_4)$ (Le Berre et al. 2007; JCPDS file 15-0756). Calculated data were obtained using Rietveld refinement of the powder pattern [*c* 6.7087(3), *b* 7.1499(2), *a* 6.9429(2) Å, β 104.442(2) °].

Single-crystal X-ray diffraction and refinement (SREF)

REE arsenates, chromates, phosphates and vanadates of $Ln(XO_4)$ type can crystallize in monoclinic (monazite structure) or tetragonal (zircon-type structure) symmetry (Botto and Baran 1982; Clavier et al. 2011; Schwarz 1963). In the REE arsenate and phosphate series, the La, Ce, Pr and Nd end-members exhibit the monazite structure (Clavier et al. 2011). REE vanadates have more complex behavior: the majority of REE vanadates (Ce–Lu, Sc) exhibit the zircon-type structure, whereas $La(VO_4)$ crystallize in both the zircon-type and monazite-type structures (Witzke et al. 2008).

The monazite-type structure was first reported by Mooney (1948) and then refined from this date by several authors for various *REE*-phosphates (Beall et al. 1981; Feigelson 1964; Ghouse 1968; Mullica et al. 1984; Mullica et al. 1985; Ni et al. 1995; Pepin and Vance

1981). The structural arrangement in monazite-type structures is based on the nine-fold coordination of the metallic cation and can be described as an equatorial pentagon interpenetrated by a tetrahedron (Clavier et al. 2011). The tetrahedron located out of the equatorial plane can then be described as a link between the REE O_9 polyhedra, leading to the formation of infinite chains along the c axis ([0 0 1] direction).

According to published data, both synthetic La(AsO_4) (Schmidt et al. 2005) and natural gasparite-(Ce) (Kolitsch et al. 2004) had a monoclinic structure with the space group $P2_1/n$.

The crystal structure of gasparite-(La) from the Wanni glacier (cotype specimen) was solved by direct methods and refined to R_1=0.014 using a *SHELX*-2015 set of programs (Scheldrick 2015) via Olex2 v.1.2.8 graphical user interface (Dolomanov et al. 2009) (Tables 6–8). Data collection and structure refinement details are given in Tables 6–7 and in the attached CIF file. The La site is coordinated by nine O atoms, with (La–O) distances of 2.586 (Table 8). The As site was found to be almost fully occupied by As ($As_{0.84}$ $P_{0.16}$), in agreement with the chemical data. The unit cell parameters (ucp) of gasparite-(La) are larger than values reported for gasparite-(Ce) (Kolitsch et al. 2004), smaller than values reported for synthetic La(AsO_4) (Schmidt et al. 2005) and in good agreement with powder XRD for the same crystal.

Electron backscatter diffraction (EBSD)

EBSD measurements were performed on an Oxford HKLNordlys Nano EBSD detector equipped on a Hitachi S-3400N scanning electron microscope. Operating conditions are listed in Table 10. Both acquisition and analysis of Kikuchi-patterns were made by Oxford AZtecHKL software. Synthetic La(AsO_4) structural data (ICSD) were used as input (Schwartz et al. 2009). The sample was polished with progressively smaller polycrystalline diamond suspensions with the ending step of Ar ion etching for 10 min at the final stage

(Oxford IonFab 300) in order remove amorphized layers for EBSD analysis. The sample was pre-tilted 70° along the normal to the EBSD detector. The fit factor (mean angular deviation (MAD)), which describes the angular deviation between the calculated and measured Kikuchi lines (good fit for deviations <1.0°) was less than 0.3° for synthetic $La(AsO_4)$ and $Ce(AsO_4)$ structures (Brahim et al. 2002; Kang and Schleid 2005; Schwartz et al. 2005).

Eighteen electron backscatter patterns from three different gasparite-(La) grains were collected (Fig. 6). Good matches were obtained for all patterns using monoclinic $La(AsO_4)$ structure with the space group $P2_1/n$ (Schmidt et al. 2005).

Discussion

Crystal chemistry and substitution mechanisms

The REE ratio in gasparite-(La) from the Ushkatyn-III deposit was stable and in all analyzed grains, La>Ce. The REE ratio in crystals of gasparite-(La) from the Wanni glacier varied significantly from Ce-dominant to La-dominant species in the same crystal (Fig. 2).

Our data revealed a very limited P-for-As substitution (P up to 0.02 apfu) and intense V-for-As substitution (V up to 0.28 apfu) in gasparite-(La) from the Ushkatyn-III deposit (Fig. 7). On the other hand, gasparite-(La) from the Wanni glacier contained no V and had intense P-for-As substitution (P up to 0.16 apfu).

Impurity of tetrahedral cations (P,V) did not appear to influence the (AsO_4) band shift as isolated tetrahedra ((AsO_4), (PO_4) and (VO_4)) in the gasparite structure surrounded by polyhedral ((LaO_9), (CeO_9), (NdO_9)). As a result, cations in the polyhedra appeared to have a major impact the position of the bands related to As-O vibrations in $(AsO_4)^{3-}$. Both P-for-As and V-for-As were reflected in the appearance of additional bands or broadening the main bands. The band around 390 cm^{-1} in the case of P-for-As (Wanni glacier), shifted upwards, and in the case of V-for-As (Ushkatyn-III deposit), downwards (Fig. 4).

No natural vanadates of monazite structure-type have been reported yet. Only

wakefieldite group minerals with the zircon structure were reported (Deliens and Piret 1986; Witzke et al. 2008). No experimental evidence for the existence of AsO_4–PO_4 substitution was reported. Cabella et al. (1999) described gasparite-(Ce) enriched with P and V and reported a wide range of V-for-As substitutions (V up to 0.30 apfu) and P-for-As substitutions (P up to 0.15 apfu). Kolitsch et al. (2004) reported that 10% of the As atoms were substituted by P (P up to 0.12 apfu) in gasparite-(Ce).

The crystal chemistry of the MXO_4 monazite-type compounds in general (*M*=La, Ce; *X*=As, P, V) have been studied intensively (e.g., Clavier et al. 2011; Kolitsch et al. 2004). Kolitsch et al. (2004) assumed that the substitution of P for As les to the substantial decrease of the *c*-parameter, which can be explained by the stacked arrangement along the [0 0 1] direction the XO_4 groups in the structure.

Our data confirmed, that both *a* and *c* ucp are influenced mainly by the size of XO_4 tetrahedra (r=0.99, r=0.92, respectively; Fig. 8a), whereas the *b* parameter is mainly influenced by the size of the MO_9 polyhedra (r=0.92; Fig. 8b).

Comparison of $LaXO_4$ monazite-type compounds showed that the (La-O) distance in MXO_4 monazite-type compounds varied significantly: 2.579 ($La(PO_4)$; Ni et al. 1995) to 2.599 Å ($La(AsO_4)$; Schmidt et al. 2005). This could explain the distortion of LaO_9 polyhedra, which is well correlated to (*X*-O) distance (r=0.99; Table 9) and could be the reason for *b vs.* (*M*-O) correlation.

Origin of gasparite-(La)

As presented above, gasparite-(La) was found in occurrence with distinct geological situations. Gasparite-(La) from the Wanni glacier, Binn Valley was found in an alpine fissure with evidence of hydrothermal alteration (well-shaped crystals in an almost empty cavity), whereas gasparite-(La) from the Ushkatyn-III deposit was found in primary Mn ores (irregular-shaped grains in calcite-rhodochrosite-fridelite veins).

We believe that in the case of gasparite-(La) from the Wanni glacier, the source of arsenic was an As-rich hydrothermal fluid, as in the case of gasparite-(Ce) (Graeser and Schwander 1987) from the same area. More challenging to explain was the source of lanthanum. The host mineral could be the main source of REE, as was shown in the case of synchisite-(Ce) (Graeser and Schwander 1987), monazite-(Ce) (Ondrejka et al. 2007) and cervandonite-(Ce) (Guastoni et al. 2013). High P content in gasparite-(La) from the Wanni glacier could indicate that monazite could be the host mineral. However, additional process of REE redistribution needed as (1) crystal of gasparite-(La) had La/Ce zoning and (2) (Ce)- and (Y)-dominant species were the rule in this region, supported by Ce/Y >> La in whole rock samples (Hofmann and Knill 1996). Another possible explanation to La-enrichment were the partial oxidation of Ce^{3+} to insoluble Ce^{4+} during fluid transportation and subsequent LREE (La, Nd, Sm) enrichment. This mechanism is well recorded in uranyl minerals (e.g., Meisser et al. 2010).

Thus, gasparite-(La) from the Wanni glacier was formed as a metasomatic mineral in the process of alteration of primary REE mineralization by As-rich hydrothermal fluid and the ensuing La/Ce separation.

The Ushkatyn-III deposit is considered as an object of hydrothermal-sedimentary genesis, transformed by processes of low-grade regional metamorphism (Brusnitsyn et al. 2018; Mitryaeva 1979; Rozhnov 1982; Skripchenko 1980).

Gasparite-(La) from the Ushkatyn-III deposit was found in microveins in hausmannite ores. It was found in association with fridelite, jacobsite, pennantite, manganhumite series minerals, sarkinite, tilasite and retzian-(La) and embedded into calcite-rhodochrosite veinlets. Similar veinlets in other rocks have a different composition. Calcite and quartz were found in microveins in the enclosing limestone. Calcite, kutnohorite, rhodonite, axinite-(Mn), friedelite, hematite, jacobsite and barite were found in microveins in braunite ores. A regular

421 change in the composition indicates the segregation mechanism of the genesis of such
422 microveins. They were formed by local redeposition of a substance from the rocks in which
423 they developed into thin cracks. Probably these processes occurred during the period of
424 tectonic deformation of the region during Late Paleozoic time.

425 We believe that As and REE were accumulated syngenetically with manganese
426 sediments in the Ushkatyn-III deposit. Most likely, the initial manganese oxides absorbed
427 these elements as it happens in modern oceans, there the absorption of REE to manganese
428 oxides occurs much more intensively than many other precipitation minerals (Dubinin 2006).

429 Occurrence of As-minerals in the Ushkatyn-III deposit is connected to the manganese
430 ores only and has not been found in the host rocks or tectonic deformation zones. Manganese
431 rocks of different genesis are often enriched in arsenic, and more than half of all discovered
432 Mn-arsenates were found in the famous Mn deposits (Abrecht 1990; Brugger and Giere 1999;
433 Brugger and Meisser 2006; Cabella et al. 1999; Frondel and Baum 1974; Holtstam and
434 Langhof 1999; Lundström 1999). Therefore, As and REE infiltration into ore layers from any
435 external source is unlikely in this case.

436 Apparently, REE and As accumulated in the initial ore-bearing sediments as a
437 component of Mn minerals. In the process of metamorphism and tectonic deformation, these
438 elements were mobilized by pore solutions and re-deposited into secant ore veins. A similar
439 mechanism for the genesis of REE-bearing arsenates is also assumed for metamorphosed Fe-
440 Mn deposits in other regions (Cabella et al. 1999; Kolitschi et al. 2004).

441 Gasparite-(La) from the Ushkatyn-III deposit is characterized by relatively small
442 amount of other REE (Ce+Nd+Pr <0.3 apfu) compared to other gasparite-(Ce) (Fig. 7) and
443 have stable La/Ce ratio. Its occurrence with retzian-(La) (Fig. 2) may indicate specific
444 conditions of mineral formation in which rocks were depleted by cerium.

445 Lanthanum and cerium have very close chemical properties, but the average content

of lanthanum in the Earth's crust is almost two times lower than cerium: 30 and 58 ppm, respectively (Li and Schoonmaker 2003). Gasparite-(La) and retzian-(La) formation require separating lanthanum from cerium. This could be done in two ways: (1) during the accumulation of manganese sediment or (2) later during lithification.

In favor of the first option is the fact that accumulations of manganese oxides of hydrothermal genesis are characterized by cerium deficiency relative to the remaining REE. In the REE spectra of such rocks, a negative cerium anomaly is usually well expressed (Dubinin 2006; Bau et al. 2014). In other words, La/Ce is higher in them than in "normal" marine sediments, which determines the possibility of the formation of lanthanum minerals. If this assumption is correct, then lanthanum minerals, including gasparite-(La) and retzian-(La), should be considered as indicators of the hydrothermal-sedimentary genesis of manganese ores. However, this issue requires further study.

According to the second option, the separation of lanthanum and cerium occurred at the post-sedimentation stage of the development of the deposit. The very low Ce content of both gasparite-(La) and retzian-(La) (less than 12 and 9 wt%, respectively) could be explained by formation from a strongly Ce-depleted source due to oxidation of Ce^{3+} and subsequent formation of insoluble cerianite-(Ce) as shown in the case of wakefieldite-(La) (Witzke et al. 2008). Cerianite-(Ce) was observed in several cases in the same samples from the Ushkatyn-III deposit where La arsenates were found. According to experimental data (Ohta, Kawabe, 2001), the oxidation of cerium with manganese oxides proceeds according to the reaction:

$$2Ce^{3+} + MnO_2 + 2H_2O = 2CeO_2 + Mn^{2+} + 4H^+$$

Reaction will shift to the right by a weak alkaline mineral formation medium, typical for carbonate associations. As a result, cerianite-(Ce) can coexist with Mn^{2+} minerals (rhodochrosite, tephroite, friedelite, etc.). However, it is possible only in the absence of

organic matter. Otherwise, there will be a dissolution of cerianite-(Ce) with the restoration of cerium by the reaction (Dubinin 2006):

$$CH_2O + 5H_2O + 11CO_2 + 4CeO_2 = 4Ce^{3+} + 12HCO_3^-$$

Accordingly, the formation of cerianite-(Ce) and, as a consequence, formation of La-rich (Ce-depleted) minerals is controlled by local distribution of Mn, REE, and organic matter.

Both scenarios considered (cerium deficiency in initial sediments and cerium concentration in cerianite-(Ce) at post-sedimentary stages) do not contradict each other. Most likely, each of them contributed to the formation of gasparite-(La) and other La-rich minerals in manganese ores of the Ushkatyn-III deposit.

Thus, gasparite-(La) from the Ushkatyn-III deposit was formed in primary ores and was not influenced by metasomatic processes. We believe that it is precisely the features of the chemical composition of the initial Mn-Fe ores that predetermined the possibility of the formation of lanthanum minerals in the Ushkatyn-III deposit.

Implications

Gasparite-(La) from Mn ores of the Ushkatyn-III deposit and metamorphic rocks of the Wanni glacier have different geological settings and different formation conditions. Thus, an occurrence of gasparite-(La) in rocks and its chemical composition could be used as a tool for geological reconstruction of their host rock formation.

In the case of gasparite-(La) from the Ushkatyn-III deposit, both REE and As were sourced from host Mn ores. In all analyzed grains, we have stable As/V/P and La/Ce ratios and As>V>P and La>Ce. Constant lanthanum predominance in analyzed gasparite grains indicate specific conditions of Mn ore formation: Ce depletion or La enrichment and no metasomatic process. Besides that, gasparite from Mn ores is characterized by low P and high V content (our data; Cabella et al. 1999). Modern metalliferous sediment is mainly composed of Fe- and Mn-oxy / hydroxides and smectite minerals (e.g., Vereshchagin et al. 2019), which

496 are carriers of V and *REE* (Emerson and Huested 1991; Gurvich, 2006). Ferromanganese ores
497 are sources of several *REE*-dominant vanadates (Moriyama et al. 2011; Witzke et al. 2008).
498 Thus, V content originated from primary Fe-, Mn- sediments and its value could be used as
499 an indicator of gasparite origin.

500 Gasparite-(La) from the Wanni glacier has different chemical features. It also has
501 stable As/V/P ratio, but in this case, As>P>V. High P content is a typical feature of gasparite
502 from metasomatic rocks (Graeser and Schwander 1987; Ondrejka et al. 2007). It also has
503 variable La/Ce ratio, which is typical for gasparite from metasomatic rocks, probably due to
504 La/Ce separation during recrystallization.

505 ## Acknowledgements

506 The work was carried out using the analytical capabilities of the Resource Centers of
507 St. Petersburg State University "X-ray Diffraction Centre," "Microscopy and microanalysis,"
508 "Innovative Technologies of Composite Nanomaterials" and "Geomodel". We are grateful to
509 Mischa Crumbach (Visp, Switzerland) for providing the picture of a gasparite-(La) crystal
510 from the Wanni glacier. We express our gratitude to A. Yu. Burkovski, Chairman of the
511 Board of Zhayremsky GOK JSC and A.V. Volkov, Chief Geologist of Zhairemsky GOK JSC
512 for assistance in the implementation of field work. Technical assistance in sample preparation
513 by D.A. Popov is highly appreciated. The authors gratefully acknowledge Dr. Evgeny V.
514 Galuskin and two anonymous reviewers for their helpful comments.

515

References list

Abrecht, J. (1990) An As-rich manganiferous mineral assemblage from the Ködnitz Valley (Eastern Alps, Austria): Geology, mineralogy, genetic considerations, and implications for metamorphic Mn deposits. Neues Jahrbuch für Mineralogie, 363-375.

Anthony, J.W., Bideaux, R.A., Bladh, K.W., and Nichols, M.C. (2000) Handbook of Mineralogy. Mineralogical Society of America.

Appiani, R., Majrani, M., and Sacchi, M. (2017) Gioielli delle Alpi italiane. Ediz. illustrata. 400 p.

Armbruster, T., Buhler, C., Graeser, S., Stalder, H.A., and Amthauer, G. (1988) Cervandonite-(Ce), (Ce,Nd,La)(Fe^{3+},Fe^{2+},Ti^{4+},Al)$_3$SiAs(Si,As)O_{13}, a new Alpine fissure mineral. Schweizerische Mineralogische und Petrographische Mitteilungen, 68, 125-132.

Barros, G., Santos, C. C., Ayala, A. P., Guedes, I., Boatner, L. A., and Loong, C.-K. (2009). Raman investigations of rare-earth arsenate single crystals. Journal of Raman Spectroscopy, 41(6), 694–697.

Bau, M., Scmidt, K., Koschinsky, A., Hein, J., Kuhn, T., and Usui, A. (2014) Discriminating between different genetic types of marine ferro-manganese crusts and nodules on rare earth elements and yttrium. Chemical Geology, 381, 1–9.

Bayliss, P., and Levinson, A.A. (1988) A system of nomenclature for rare-earth mineral species: Revision and extension. American Mineralogist, 73, 422-423.

Beall, G.W., Boatner, L.A., Mullica, D.F., and Milligan, W.O. (1981) The structure of cerium ortho-phosphate, a synthetic analog of monazite. Journal of Inorganic and Nuclear Chemistry, 43, 101–5.

Bedlivy, D., and Mereiter, K. (1982) Structure of α-$BiAsO_4$ (rooseveltite), Acta Crystallographica, B38, 1559-1561.

Bergomi, M. A., Dal Piaz, G. V., Malusà, M. G., Monopoli, B., and Tunesi, A. (2017)

The Grand St Bernard-Briançonnais nappe system and the Paleozoic inheritance of the Western Alps unraveled by zircon U-Pb dating. Tectonics, 36, 2950–2972.

Botto, I. L., and Baran, E. J. (1982) Characterization of the monoclinic rare earth orthoarsenates. Journal of the Less Common Metals, 83, 255-261.

Brahim, A. Mongi, F. M., and Amor, H. (2002) Cerium arsenate, $CeAsO_4$. Acta Crystallographica, E58, 98-99.

Breiter, K., Čopjaková, R., and Škoda, R. (2009) The involvement of F, CO2, and As in the alteration of Zr-Th-REE-bearing accessory minerals in the Hora Svaté Kateřiny A-type granite, Czech Republic. Canadian Mineralogist, 47, 1375-1398.

Brugger, J., and Meisser, N. (2006) Manganese-rich assemblages in the Barrhorn unit, Turtmanntal, central Alps, Switzerland. Canadian Mineralogist, 44, 229-248.

Britvin, S.N., Dolivo-Dobrovolsky, D.V., and Krzhizhanovskaya, M.G. (2017) Software for processing the X-ray powder diffraction data obtained from the curved image plate detector of Rigaku RAXIS Rapid II diffractometer. Proceedings of the Russian Mineralogical Society, 146, 3, 104–107.

Brugger, J., and Giere, R. (1999) As, Sb, Be and Ce enrichment in minerals from a metamorphosed Fe–Mn deposits, Val Ferrera, Eastern Swiss Alps. Canadian Mineralogist, 37, 37–52.

Brusnitsyn, A.I., Perova, E.N., Vereshchagin, O.S., Letnikova, E.F., Shkolnik, S.I., and Ivanov, A.V. (2017) Stratiform lead-zinc and iron-manganese ores of the Zhayremsky ore cluster (Central Kazakhstan): conditions of occurrence, composition, genesis. Metallogeny of ancient and modern oceans. Differentiation and reasons for the diversity of ore deposits. Miass: IMIN UB RAS, 90-94. (in Russian)

Brusnitsyn, A.I., Perova, E.N., Vereshchagin, O.S., Britvin, S.N., Platonova, N.V., and Shilovskikh, V.V. (2018) Genetic mineralogy of manganese ores of Ushkatyn-III deposit,

566 Central Kazakhsan. Metallogeny of ancient and modern oceans. Volcanism and ore
567 formation. Miass: IMIN UB RAS, 67-70. (in Russian)

568 Buzmakov, E.I., Shibrik, V.I., Rozhnov, A.A., Sereda, V.Ya., and Radchenko, N.M.
569 (1975) Stratiform iron-manganese and polymetallic deposits of the Ushkatynsky ore field
570 (Central Kazakhstan). Geology of ore deposits, 1, 32–46. (in Russian)

571 Cabella, R., Lucchetti, G., and Marescotti, P. (1999) Occurrence of *LREE*- and Y-
572 arsenates from a Fe-Mn deposit, Ligurian Briançonnais Domain, Maritime Alps, Italy.
573 Canadian Mineralogist, 37, 961-972.

574 Campbell, K.M., and Nordstrom, D.K. (2014) Arsenic speciation and sorption in
575 natural environments. Reviews in Mineralogy and Geochemistry, 79, 185-216.

576 Clavier, N., Podor, R., and Dacheux, N. (2011) Crystal chemistry of the monazite
577 structure. Journal of the European Ceramic Society, 31, 941-976.

578 Cuchet, S., van der Burgt, A. and Meisser, N. (2005) Chummibort, eine neue
579 Fundstelle für Arsenmineralien im Binntal. Schweizer Strahler, 2, 19-29.

580 Cuchet, S., Crumbach, M., and van der Burgt, A. (2014) Das Binntal enthüllt ein
581 grosses Geheimnis. Le Binntal nous dévoile un grand secret. Schweizer Strahler, 48, 2, 2 –
582 55.

583 Cuchet, S., Crumbach, M., and van der Burgt, A. (2016) Le allaniti e i minerali di
584 terre rare dell'Alpe Veglia (Varzo, Verbano-Cusio-Ossola). Rivista Mineralogica Italiana, 40,
585 4, 212 – 24.

586 Deliens, M., and Piret, P. (1986) Kusuite becomes plombean wakefieldite (Ce).
587 Bulletin de Mineralogie, 109(3), 305.

588 Demartin, F., Gramaccioli, C.M., and Pilati, T. (1994) Paraniite-(Y), a new tungstate
589 arsenate mineral from Alpine fissures. Schweizerische Mineralogische und Petrographische
590 Mitteilungen, 74, 155-160.

591 Dolomanov, O.V., Bourhis, L.J., Gildea, R.J., Howard, J.A., and Puschmann H.
592 (2009) OLEX2: a complete structure solution, refinement and analysis program. Journal of
593 Applied Crystallography, 42, 339-341.
594 Dubinin, A.V. (2006) Geochemistry of Rare Earth Elements in the Ocean. Moscow,
595 Nauka Publ. 359 p. (in Russian)
596 Dunn, P. J., Peacor, D.R., and Simmons, W. B. (1984) Retzian-(La), a new mineral
597 from Sterling Hill, Sussex County, New Jersey. Mineralogical Magazine, 48, 533-535.
598 Feigelson, R.S. (1964) Synthesis and single-crystal growth of rare-earth
599 orthophosphates. Journal of the American Ceramic Society, 47, 257–8.
600 Foord, E.E., Hughes, J.M., Cureton, F., Maxwell, C.H., Flaster, A.U., Sommer, A.J.,
601 and Hlava, P.F. (1999) Esperanzaite, $NaCa_2Al_2(As^{5+}O_4)_2F_4(OH)\cdot 2H_2O$, a new mineral
602 species from the La Esperanza Mine, Mexico: Descriptive mineralogy and atomic
603 arrangement. Canadian Mineralogist, 37, 67-72.
604 Förster, H.-J., Ondrejka, M., and Uher, P. (2011) Mineralogical responses to
605 subsolidus alteration of granitic rocks by oxidizing As-bearing fluids: REE arsenates and As-
606 rich silicates from the Zinnwald granite, eastern Erzgebirge, Germany. Canadian
607 Mineralogist, 49, 913-930.
608 Frondel, C., and Baum, J. (1974) Structure and mineralogy of the Franklin zinc-iron-
609 manganese deposit, New Jersey. Economic Geology, 69, 157-180.
610 Gatta, D. G., Rotiroti, N., Cámara, F., and Meven, M. (2018) On the labyrinthine
611 world of arsenites: a single-crystal neutron and X-ray diffraction study of cafarsite. Physics
612 and Chemistry of Minerals, 45, 9, 819–829.
613 Giera, A., Manecki, M., Bajda, T., Rakovan, J., Kwaśniak-Kominek, M., and
614 Marchlewski, T. (2016) Arsenate substitution in lead hydroxyl apatites: A Raman
615 spectroscopic study. Spectrochimica Acta Part A: Molecular and Biomolecular Spectroscopy,

152, 370-377.

Graeser, S. (1966) Asbecasit und Cafarsit, zwei neueMineralien aus dem Binnatal (Kt. Wallis). Schweizerische Mineralogische und Petrographische Mitteilungen, 46, 367-375.

Graeser, S., and Roggiani, A.G. (1976) Occurrence and genesis of rare arsenate and phosphate minerals around Pizzo Cervandone, Italy/Switzerland. Rendicontri della Societa Italiana di Mineralogia e Petrologia, 32, 279–288.

Graeser, S., and Schwander, H. (1987) Gasparite-(Ce) and monazite-(Nd): two new minerals to the monazite group from the Alps. Schweizerische Mineralogische und Petrographische Mitteilungen, 67, 101-113.

Graeser, S., Schwander, H., Demartin, F., Gramaccioli, C.M., Pilati, T. and Reusser, E. (1994) Fetiasite (Fe^{2+}, Fe^{3+},Ti)$_3O_2[As_2O_5]$, a new arsenite mineral: its description and structure determination. American Mineralogist, 79, 996-1002.

Ghouse, K.M. (1968) Refinement of crystal structure of heat-treated monazite crystal. Indian Journal of Pure and Applied Physics, 6, 265–8.

Guastoni, A., Pezzota, F., and Vignola, P. (2006) Characterization and genetic inferences of arsenates, sulfates and vanadates of Fe, Cu, Pb, Zn from Mount Cervadone (Western Alps, Italy). Periodico di Mineralogia, 75, 141–150.

Guastoni, A., Nestola, F., Gentile, P., Zorzi, F., Alvaro, M., Lanza, A., Peruzzo, L., Schiazza, M., and Casati, N. M. (2013) Deveroite-(Ce): a new REE-oxalate from Mount Cervandone, Devero Valley, Western-Central Alps, Italy. Mineralogical Magazine, 77, 3019-3026.

Gurvich, E. G. (2006) Metalliferous sediments of the world ocean. Fundamental theory of deep-sea hydrothermal sedimenta-tion. Springer, Heidelberg, 416p.

Hettmann, K., Kreissig, K., Rehkämper, M., Wenzel, T., Mertz-Kraus, R., and Markl, G. (2014) Thallium geochemistry in the metamorphic Lengenbach sulfide deposit,

641 Switzerland: Thallium-isotope fractionation in a sulfide melt. American Mineralogist, 99, 4,
642 793-803.

643 Hofmann, B., and Knill, M.D. (1996) Geochemistry and genesis of the Lengenbach
644 Pb-Zn-As-Tl-Ba-mineralisation, Binn Valley, Switzerland. Mineralium Deposita, 31, 319–
645 339.

646 Holtstam, D., and Langhof, J. (editors) Langban, the Mines, their minerals, histoty
647 and explorers. Raster Forlag, Stockholm, 1999. 215 p.

648 JSC "Zhayremsky ore mining and processing enterprise". Annual report for the year
649 2015. Publishing house JSC ZHGOK: 2015. 103 p. (in Russian)

650 Kang, D. - H., and Schleid, T. (2005) Einkristalle von La[AsO_4] im Monazit - und
651 Sm[AsO4] im Xenotim - Typ. Zeitschrift fuer Anorganische und Allgemeine Chemie, 631,
652 10, 1799-1802.

653 Kayupova, M.M. (1974) Mineralogy of iron and manganese ores of the Western
654 Atasu (Central Kazakhstan). Alma-Ata, Nauka, 232 p. (in Russian)

655 Klemm, L., Pettke, T., Graeser, S., Mullis, J., and Kouzmanov, K. (2004) Fluid
656 mixing as the cause of sulphide precipitation at Albrunpass, Binn Valley, Central Alps.
657 Schweizerische Mineralogische und Petrographische Mitteilungen, 84, 189–212.

658 Kolitsch, U, and Holtstam, A. (2004) Crystal chemistry of *REEX*O_4 compounds (*X* =
659 P, As, V). II. Review of *REEX*O_4 compounds and their stability fields. European Journal of
660 Mineralogy, 16, 117–126.

661 Kolitsch, U., Holtstam, D., and Gatedal, K. (2004) Crystal chemistry of *REEX*O_4
662 compounds (*X* = P, As, V). I. Paragenesis and crystal structure of phosphatian gasparite-(Ce)
663 from the Kesebol Mn-Fe-Cu deposit, Västra Götaland, Sweden. European Journal of
664 Mineralogy, 16, 111-116.

665 Krzemnicki, M. (1992) As-Bi-Mineralisationen in der Monte-Leone-Decke im

Mättital (Binntal-Region). Thesis, Universität Basel, Switzerland, 122 p.

Krzemnicki, M. (1997) Mineralogical investigations on hydrothermal As- and REE-bearing minerals within the gneisses of the Monte-Leone nappe (Binntal region, Switzerland). Dissertation, Universität Basel, Switzerland, 86 p.

Krzemnicki, M.S., and Reusser, E. (1998) Graeserite, $Fe^{3+}_4Ti_3As^{3+}O_{13}(OH)$ a new mineral species of the derbylite group from from the Mount Leone Nappe, Binntal Region, Western Alps, Switzerland. Canadian Mineralogist: 36: 1083-1088.

Le Berre, J.-F., Gauvin, R., and Demopoulos, G. P. (2007) Synthesis, Structure, and Stability of Gallium Arsenate Dihydrate, Indium Arsenate Dihydrate, and Lanthanum Arsenate. Industrial and Engineering Chemistry Research, 46, 7875-7882.

Li, Y.-H., and Schoonmaker, J.E. (2003) Chemical composition and mineralogy of marine sediments. Treatise on Geochemistry. Sediments, diagenesis, and sedimentary rocks, 7, 1–35.

Lundström, I. (1999) General geology of the Bergslagen ore region. In: Långban. The Mines, Their Minerals,Geology and Explorers. Holtstam D, Langhof J (ed) Christian Weise Verlag, 19-27.

Mancini, S. (2000) Le mineralizzazioni a manganese delle Alpi Apuane. Tesi di Laurea, University of Pisa.

Majzlan, J., Drahota, P., and Filippi, M. (2014) Parageneses and crystal chemistry of arsenic minerals. Reviews in Mineralogy and Geochemistry, 79, 17–184.

Maynard, J.B. (2003) Manganiferous sediments, rocks and ores. Treatise on Geochemistry. Sediments, diagenesis, and sedimentary rocks, 7, 289–308.

Maxelon, M., and Mancktelow, N. S. (2005) Three-dimensional geometry and tectonostratigraphy of the Pennine zone, Central Alps, Switzerland and Northern Italy. Earth Science Reviews, 71, 171–227.

Meisser, N., Brugger, J., Ansermet, S., Thelin, P., and Bussy, F. (2010). Francoisite-(Ce), a new mineral species from La Creusaz uranium deposit (Valais, Switzerland) and from Radium Ridge (Flinders Ranges, South Australia): Description and genesis. American Mineralogist, 95(10), 1527 - 1532.

Mills, S., Kartashov, P. M., Kampf, A. R., and Raudsepp, M. (2010) Arsenoflorencite-(La), a new mineral from the Komi Republic, Russian Federation: description and crystal structure. European Journal of Mineralogy, 22, 613-621.

Mitryaeva, N.M. (1979) Mineralogy of barite-zinc-lead ores of Atasuisky district. Alma-Ata, Nauka, 219 p. (in Russian)

Modresky, P.J. (1983) Agardite-(La), a chemically complex rare-earth arsenate from the gallinas district, Lincoln Co., New Mexico. In Anthony, J. W., (editor), Oxidation Mineralogy of Base Metal Deposits, Fifth Joint Mineralogical Society of America - Friends of Mineralogy Symposium.

Mooney, R.C.L. (1948) Crystal structures of a series of rare earth phosphates. The Journal of Chemical Physics 16, 1003.

Moralev, G.V., Borisov, A.V., Surenkov, S.V., Nagaeva, S.P., Tarbaev, M. B., Kuznetsov, S. K., Onishchenko, S. A., Efanova, L. I., and Soboleva, A. A. (2005) Distribution and Modes of Occurrence of REE at the Chudnoe and Nesterovskoe Occurrences of Au–Pd–REE Ore Mineralization in the Maldynyrd Range, Nether-Polar Urals. Geochemistry International, 43, 11, 1078–1097.

Moriyama, T., Miyawaki, R., Yokoyama, K., Matsubara, S., Hirano, H., Murakami, H., and Watanabe, Y. (2011) Wakefieldite-(Nd), a new neodymium vanadate mineral in the Arase stratiform ferromanganese deposit, Kochi Prefecture, Japan. Resource Geology 61, 101-110.

Mullica, D.F., Milligan, W.O., Grossie, D.A., Beall, G.W., and Boatner, L.A. (1984)

716 Ninefold coordination in $LaPO_4$—pentagonal interpenetrating tetrahedral polyhedron.
717 Inorganica Chimica Acta, 95, 231–6.

718 Mullica, D.F., Grossie, D.A, and Boatner, L.A. (1985) Structural refinements of
719 praseodymium and neodymium ortho-phosphate. Journal of Solid State Chemistry, 58, 71–7.

720 Ni, Y., Hughes, J. M., and Mariano, A. N. (1995) Crystal chemistry of the monazite
721 and xenotime structures. American Mineralogist, 80, 21-26.

722 Ondrejka, M., Uher, P., Pršek, J., and Ozdín, D. (2007) Arsenian monazite-(Ce) and
723 xenotime-(Y), *REE* arsenates and carbonates from the Tisovec-Rejkovo rhyolite, Western
724 Carpathians, Slovakia: Composition and substitutions in the (*REE*,Y)XO$_4$ system (X = P, As,
725 Si, Nb, S). Lithos, 95, 116–129.

726 Pepin, G.J., and Vance, E.R. (1981) Crystal data for rare earth orthophosphates of the
727 monazite structure-type. Journal of Inorganic and Nuclear Chemistry, 43(II), 2807–9.

728 Raison, P.E., Jardin, R., Bouexiere, D., Konings, R.J.M., Geisler, T., Pavel, C.C.,
729 Rebizant, J., and Popa, K. (2008) Structural investigation of the synthetic CaAn $(PO_4)_2$ (An =
730 Th and Np) cheralite-like phosphates. Physics and Chemistry of Minerals, 35, 603-609.

731 Roth, P., and Meisser, N. (2013) Die seltenen Mineralien der Büdner
732 Manganvorkommen. Schweizer Strahler, 47, 3, 8-21.

733 Rozhnov, A.A. (1982) Comparative characteristics of manganese deposits of
734 Atasuisky and Nikopol-Chiatura types. In: Geology and geochemistry of manganese,
735 Moscow, Nauka, 116–121. (in Russian)

736 Schwarz, H. (1963) The phosphates, arsenates, and vanadates of the rare earths.
737 Zeitschrift für anorganische und allgemeine Chemie, 323, 44-56.

738 Schwartz, A. J., Kumar, M., Adams, B. L. Electron Backscatter Diffraction in
739 Materials Science, Springer, New York, 2009.

740 Schmidt, M., Müller, U., Cardoso-Gil, R., Milke, E., and Binnewies, M. (2005) Zum

741 Chemischen Transport und zur Kristallstruktur von Seltenerdarsenaten(V). Zeitschrift für
742 anorganische und allgemeine Chemie, 631, 1154-1162.

743 Scheldrick, G.M. (2015) Crystal structure refinement with SHELXL. Acta
744 Crystallographica, C71, 3-8.

745 Skripchenko, N.S. (1980) Hydrothermal-sedimentary polymetallic ores of calc-slate
746 formations. Moscow, Nedra, 215 p. (in Russian)

747 Skripchenko, N.S. (1989) Forecasting deposits of non-ferrous metals in sedimentary
748 rocks. Irkutsk, Nedra, 207 p. (in Russian)

749 Solecka, U., Bajda, T., Topolska, J., Zelek-Pogudz, S., and Manecki, M. (2018)
750 Raman and Fourier transform infrared spectroscopic study of pyromorphite-vanadinite solid
751 solutions. Spectrochimica Acta Part A: Molecular and Biomolecular Spectroscopy, 190, 96–
752 103.

753 Song, H., Liub, J., and Cheng, H. (2018) Structural and spectroscopic study of
754 arsenate and vanadate incorporation into apatite group: Implications for semi-quantitative
755 estimation of As and V contents in apatite. Spectrochimica Acta Part A: Molecular and
756 Biomolecular Spectroscopy, 188, 488–494.

757 Stoe, Cie (2006) WinXPOW v. 1.07. Stoe & Cie, Darmstadt, Germany.

758 Streckeisen, A., Wenk, E., and Frey, M. (1974): On steep isogradic surfaces in the
759 Simplon area. Contributions to Mineralogy and Petrology, 47, 8l-95.

760 Steck, A. (1987) Le massif du Simplon. Reflexions sur la cinematique des nappes de
761 gneiss. Schweizerische Mineralogische und Petrographische Mitteilungen. 67, 27-45.

762 Vereshchagin, O. S., Perova, E.N., Brusnitsyn, A. I., Ershova, V. B., Khudoley, A. K.,
763 Shilovskikh, V. V., Molchanova, E. V. (2019) Ferro-manganese nodules from the Kara Sea:
764 Mineralogy, geochemistry and genesis. Ore Geology Reviews. 106, 192–204.

765 Witzke, T., Kolitsch, U., Warnsloh, J.M., and Göske, J. (2008) Wakefieldite-(La), a

766 new mineral species from the Glücksstern Mine, Friedrichroda, Thuringia, Germany.
767 European Journal of Mineralogy, 20, 1135-1139.

768 Wu, Y., Kukkadapu, R. K., Livi, K. J. T., Xu, W., Li, W., and Sparks, D. L. (2018)
769 Iron and arsenic speciation during As(III) oxidation by manganese oxides in the presence of
770 Fe(II): molecular-level characterization using XAFS, Mössbauer, and TEM analysis. ACS
771 Earth and Space Chemistry, 2, 256−268.

772 Yang, H., Downs, R.T., Jenkins, R.A., and Evans, S.H. (2018): Segerstromite,
773 $Ca_3(As^{5+}O_4)_2[As^{3+}(OH)_3]_2$, the first mineral containing $As^{3+}(OH)_3$, the arsenite molecule,
774 from the Cobriza mine in the Atacama Region, Chile. American Mineralogist, 103, 1497–
775 1501.

776

777 **Figure captions**

778 Figure 1. Morphology of gasparite-(La): (a) irregular-shaped grains and aggregates in calcite
779 veins from the Ushkatyn-III deposit (BSE image), (b) elongated crystal (yellow) with albite
780 crystals (white) from the Wanni glacier (optical microscopy). Note: gasparite-(La)-Gas,
781 jacobsite-Jac, retzian-(La)-Ret, alleghanyite-All, calcite-Cal.

782 Figure 2. Chemical zoning of gasparite crystal from the Wanni glacier

783 Figure 3. Reflectance spectra in air for gasparite-(La) from the Ushkatyn-III deposit.

784 Figure 4. Raman spectra in air for gasparite-(La) from the Ushkatyn-III deposit, gasparite-
785 (La) from the Wanni glacier and synthetic La(AsO_4) (Botto and Baran, 1982)

786 Figure 5. (a) EBSB pattern of the gasparite-(La) crystal taken (30 kV accelerating voltage,
787 0.3 nA beam current, 5 seconds exposure per frame, averaging of 20 frames, 1344x1024
788 pixels image size), and (b) the pattern indexed with the $P2_1/n$ structure (MAD 0.15, 80 bands
789 are represented on an image)

790 Figure 6. Chemical composition variations in gasparite group minerals: (a) La-Ce-Nd ratio,
791 (b) As-V-P ratio

792 Figure 7. As vs. V+P+S substitution

793 Figure 8. Unit cell parameters of $M(XO_4)$ compounds (M=La, Ce; X=As, P, V): (a) c vs. (X-
794 O), (b) b vs. (M-O)

795

This is a preprint, the final version is subject to change, of the American Mineralogist (MSA)
Cite as Authors (Year) Title. American Mineralogist, in press.
DOI: https://doi.org/10.2138/am-2019-7028

796

797 Table 1. Chemical composition of gasparite-(La)

Constituent	Ushkatyn-III deposit		Wanni glacier	
	Wt%	**Range**	**Wt%**	**Range**
Fe_2O_3	0.05	0.00-0.16	0.00	0.00
MnO	1.30	0.91-1.96	0.00	0.00
CaO	1.33	0.97-1.54	0.34	0.24-0.48
ThO_2	0.00	0.00	0.58	0.37-0.72
Y_2O_3	0.01	0.00-0.05	0.01	0.00-0.03
La_2O_3	40.21	37.83-41.17	35.59	34.57-36.74
Ce_2O_3	10.69	9.76-11.61	22.55	21.26-23.67
Pr_2O_3	1.46	0.00-1.99	0.29	0.00-0.88
Nd_2O_3	4.24	3.53-4.69	1.04	0.50-1.30
Sm_2O_3	0.09	0.00-0.33	0.07	0.00-0.35
V_2O_5	9.77	8.58-11.21	0.00	0.00
P_2O_5	0.64	0.22-0.99	4.29	4.18-4.45
As_2O_5	30.32	29.46-31.41	34.48	33.27-35.22
Total	**100.11**		**100.13**	

798

This is a preprint, the final version is subject to change, of the American Mineralogist (MSA)
Cite as Authors (Year) Title. American Mineralogist, in press.
DOI: https://doi.org/10.2138/am-2019-7028

799 Table 2. Comparative crystallographic data for monazite group minerals

Mineral	Gasparite-(La)	Gasparite-(Ce)	Rooseveltite	Monazite-(La)	Monazite-(Ce)	Monazite-(Nd)	Monazite-(Sm)	Cheralite
Chemical formula	$La(AsO_4)$	$Ce(AsO_4)$	$Bi(AsO_4)$	$La(PO_4)$	$Ce(PO_4)$	$Nd(PO_4)$	$Sm(PO_4)$	$CaTh(PO_4)_2$
Crystal system	Monoclinic							
Space group	$P2_1/n$							
a (Å)	6.9576(4)	6.929(3)	6.879(1)	6.8313(10)	6.7880(10)	6.7352(10)	6.6818(12)	6.7085(8)
b (Å)	7.1668(4)	7.129(3)	7.159(1)	7.0705(9)	7.0163(9)	6.9500(9)	6.8877(9)	6.4152(6)
c (Å)	6.7155(4)	6.697(3)	6.732(1)	6.5034(9)	6.4650(7)	6.4049(8)	6.3653(9)	6.4152(6)
β (°)	104.414(1)	104.46(3)	104.84(1)	103.27(1)	103.43(1)	103.68(1)	103.86(1)	103.71(1)
Z	4							
Reference	Our data	Kolitsch et al. 2004	Bedlivy and Mereiter 1982	Ni et al. 1995				Raison et al. 2008

800

801

This is a preprint, the final version is subject to change, of the American Mineralogist (MSA)
Cite as Authors (Year) Title. American Mineralogist, in press.
DOI: https://doi.org/10.2138/am-2019-7028

802 Table 3. Reflectance of gasparite-(La) from the Ushkatyn-III deposit measured in air

λ (nm)	**R_1**	**R_2**	**λ (nm)**	**R_1**	**R_2**
400	11.19	9.05	**560**	10.92	8.90
420	12.04	9.82	**580**	10.88	8.84
440	12.35	10.15	**589**	10.87	8.83
460	12.35	10.13	**600**	10.85	8.81
470	12.16	9.95	**620**	10.85	8.77
480	11.97	9.77	**640**	10.89	8.74
500	11.45	9.44	**650**	10.92	8.77
520	11.15	9.17	**660**	10.94	8.79
540	11.00	9.00	**680**	11.09	8.86
546	10.98	8.98	**700**	11.23	9.08

803

804 Table 4. Raman spectral signatures of gasparite-(La)

Raman shift, cm^{-1} / Relative Intensity			**Assignment**	**Raman shift (cm^{-1}) / Relative Intensity**			**Assignment**
Ushkatyn-III	Wanni glacier	Botto and Baran 1982		Ushkatyn-III	Wanni glacier	Botto and Baran 1982	
92 / vw	94 / vw		Lattice vibrations	364 / vw	367 / w	350 / vw 367 / w	$v_4(AsO_4)$
104 / vw	107 / w						
126 / vw	125 / w			379 / st	395/ st	392 / m	$v_2(AsO_4)$
138 / vw	139 / vw						
153 / vw	155 / w			422 / w 452 / w	421 / m 462 / w	418 / w 440 / sh 461 / w	$v_4(AsO_4)$
190 / vw	190 / w						
203 / m	203 / vw						
264 / vw	267 vw			822 / m 843 / sh	812 / sh 826 / sh 848 / sh	798 / vw 827 / m 845 / st 872 / sh	$v_3(AsO_4)$
320 / w		322 / w					
334 / vw	337 / w	336 / w					
				860 / vs	864 / vs	861 / vs	$v_1(AsO_4)$
					951 / w		$v_1(PO_4)$

805 Note: Vs – very strong; st – strong; m – medium; w – weak; vw – very weak; sh –shoulder.
806

807

This is a preprint, the final version is subject to change, of the American Mineralogist (MSA)
Cite as Authors (Year) Title. American Mineralogist, in press.
DOI: https://doi.org/10.2138/am-2019-7028

808 Table 5. Powder X-ray diffraction data for gasparite-(La) from the Wanni glacier

I_{obs}	d_{obs}	I_{calc}	d_{calc}	*h*	*k*	*l*		I_{obs}	d_{obs}	I_{calc}	d_{calc}	*h*	*k*	*l*
9	5.39	5	5.39	1	0	-1		**19**	1.898	13	1.900	0	2	3
13	4.89	10	4.90	0	1	1		**6**	1.851	3	1.853	3	2	0
12	4.80	9	4.81	1	1	0		**19**	1.814	19	1.816	2	-2	-3
12	4.30	10	4.31	1	-1	-1				2	1.794	1	3	2
8	4.18	3	4.18	1	0	1				5	1.789	0	4	0
		5	3.61	1	1	1		**25**	1.780	22	1.780	2	3	1
20	3.574	16	3.577	0	2	0		**11**	1.727	10	1.728	0	4	1
64	3.361	58	3.363	0	0	2				3	1.681	0	0	4
6	3.249	5	3.249	2	0	0		**9**	1.673	8	1.673	2	0	-4
100	3.156	100	3.158	0	2	1				7	1.637	0	1	4
22	3.042	18	3.043	0	1	2		**17**	1.633	5	1.633	0	3	3
		26	2.968	2	-1	-1				2	1.633	4	-1	-1
77	2.956	69	2.958	2	1	0				2	1.631	4	0	-2
24	2.693	22	2.695	2	0	-2				5	1.624	4	0	0
19	2.519	18	2.524	2	-1	-2		**8**	1.619	3	1.618	2	1	3
19	2.511	12	2.506	2	1	1		**8**	1.587	6	1.590	4	-1	-2
8	2.446	5	2.450	0	2	2				2	1.584	4	1	0
6	2.407	6	2.410	2	-2	-1		**12**	1.579	5	1.579	2	-3	-3
5	2.301	3	2.304	1	0	-3				3	1.579	0	4	2
16	2.233	8	2.239	1	3	0		**7**	1.517	5	1.519	4	-2	-1
		8	2.230	3	0	-1				2	1.494	3	2	2
12	2.189	8	2.193	1	-1	-3		**6**	1.491	2	1.491	2	-4	-2
11	2.163	6	2.166	1	2	2		**4**	1.473	2	1.474	4	-1	-3
8	2.138	3	2.139	0	1	3		**6**	1.397	3	1.398	0	4	3
		2	2.021	2	-1	-3		**10**	1.379	8	1.380	4	2	1
33	2.004	31	2.006	2	1	2		**8**	1.374	6	1.372	4	-3	-1
9	1.941	4	1.942	1	-3	-2		**15**	1.362	3	1.364	2	-4	-3
30	1.923	28	1.925	2	-3	-1								

809

810

This is a preprint, the final version is subject to change, of the American Mineralogist (MSA)
Cite as Authors (Year) Title. American Mineralogist, in press.
DOI: https://doi.org/10.2138/am-2019-7028

Table 6. Crystal data, collection and structure refinement details for gasparite-(La) from the Wanni glacier

Crystal Data	
Chemical formula	$(La_{0.60}Ce_{0.40})((As_{0.84}P_{0.16})O_4)$
M_r	271.39
Crystal system, space group	Monoclinic, $P2_1/n$
a, b, c (Å)	6.7155 (4), 7.1668 (4), 6.9576 (4)
β (°)	104.414 (1)
V (Å^3)	324.32 (3)
Z	4
D_x (g/cm^3)	5.558
Crystal size (mm)	0.04 × 0.04 × 0.03
Data collection	
Diffractometer	Bruker *APEX*-II CCD
Radiation type	Mo$K\alpha$ (0.71073 Å)
μ (mm^{-1})	21.95
Absorption correction	Multi-scan
No. of measured, independent and observed [$I > 2s(I)$] reflections	3839, 944, 869
2Θ range for data collection (°)	7.55 to 60.00
Index ranges	$-9 \le h \le 9$, $-9 \le k \le 10$, $-9 \le l \le 9$
Refinement	
R_{int}, R_σ	0.0207, 0.0175
$R_1[F^2 > 2\sigma(F^2)]$, $wR_2(F^2)$, S	0.014, 0.029, 1.12
No. of reflections	944
No. of parameters	57
$\Delta\rho_{max}$, $\Delta\rho_{min}$ (e Å^{-3})	0.76, -0.55

Table 7. Fractional atomic coordinates and isotropic displacement parameters (U_{iso}, Å^2) for gasparite-(La) from the Wanni glacier

Site	***x***	***y***	***z***	U_{iso}	**Occupancy (<1)**
M (4*e*)	0.40018 (2)	0.34494 (2)	0.21899 (2)	0.00827 (6)	$(La_{0.6}Ce_{0.4})$ *
X (4*e*)	0.38653 (4)	0.16300 (4)	0.69644 (4)	0.00626 (11)	$(As_{0.84}P_{0.16})$
O1 (4*e*)	0.2803 (3)	0.2142 (3)	0.8797 (3)	0.0131 (4)	
O2 (4*e*)	0.5664 (3)	-0.0012 (3)	0.7481 (3)	0.0133 (4)	
O3 (4*e*)	0.5031 (3)	0.3390 (3)	0.6113 (3)	0.0122 (4)	
O4 (4*e*)	0.1793 (3)	0.1075 (3)	0.5181 (3)	0.0130 (4)	

Note:* Occupancy of *M* site was fixed according to electron microprobe data.

This is a preprint, the final version is subject to change, of the American Mineralogist (MSA)
Cite as Authors (Year) Title. American Mineralogist, in press.
DOI: https://doi.org/10.2138/am-2019-7028

818 Table 8. Anisotropic displacement parameters (Å^2) for gasparite-(La) from the Wanni glacier

Site	U^{11}	U^{22}	U^{33}	U^{12}	U^{13}	U^{23}
M	0.00902 (8)	0.00690 (9)	0.00836 (8)	0.00092 (6)	0.00117 (5)	0.00025 (6)
X	0.00599 (16)	0.00562 (17)	0.00700 (16)	-0.00001 (11)	0.00131 (11)	0.00013 (11)
O1	0.0119 (10)	0.0165 (11)	0.0105 (9)	-0.0006 (8)	0.0024 (8)	-0.0027 (8)
O2	0.0108 (10)	0.0086 (10)	0.0199 (10)	-0.0009 (8)	0.0029 (8)	-0.0012 (8)
O3	0.0162 (10)	0.0097 (10)	0.0117 (9)	-0.0033 (8)	0.0054 (8)	0.0009 (8)
O4	0.0119 (10)	0.0131 (11)	0.0120 (9)	0.0002 (8)	-0.0011 (8)	-0.0048 (8)

819

820 Table 9. Selected bond lengths (Å) and distortion of *M*-polyhedra for gasparite-(La)
821 from the Wanni glacier and structurally related $M(XO_4)$ compounds (*M*=La, Ce; *X*=As, P, V).

Bond	**Length**					
	Gasparite-(La)	Gasparite-(Ce)	$La(AsO_4)$	$Ce(AsO_4)$	$La(VO_4)$	$La(PO_4)$
M—O1^{iii}	2.554 (2)	2.486(5)	2.571(3)	2.939(8)	2.521(4)	2.479(3)
M —O1^{iv}	2.481 (2)	2.527(5)	2.489(3)	2.636(9)	2.497(3)	2.554(3)
M —O2^{v}	2.479 (2)	2.902(5)	2.498(4)	2.460(7)	2.656(3)	2.783(3)
M —O2^{ii}	2.559 (2)	2.544(4)	2.560(4)	2.619(8)	2.568(3)	2.589(3)
M —O3^{ii}	2.901 (2)	2.632(5)	2.655(3)	2.472(8)	2.528(4)	2.615(3)
M —O3^{vi}	2.562 (2)	2.620(6)	2.577(3)	2.551(7)	2.677(4)	2.503(3)
M —O3	2.6440 (19)	2.457(5)	2.912(4)	2.562(7)	2.887(4)	2.672(3)
M —O4^{iii}	2.624 (2)	2.488(5)	2.644(4)	2.476(7)	2.533(4)	2.466(3)
M —O4^{vii}	2.472 (2)	2.555(4)	2.486(3)	2.543(7)	2.502(4)	2.548(3)
(*M*-O)	*2.586*	*2.579*	*2.599*	*2.584*	*2.597*	*2.579*
Δ*M*	*0.035*	*0.036*	*0.035*	*0.038*	*0.037*	*0.030*
X—O1	1.650 (2)	1.647(5)	1.670(4)	1.682(8)	1.724(4)	1.523(3)
X—O2	1.660 (2)	1.664(5)	1.680(4)	1.699(7)	1.720(4)	1.553(3)
X—O3	1.669 (2)	1.659(5)	1.695(4)	1.692(7)	1.699(4)	1.541(3)
X—O4	1.6656 (19)	1.615(5)	1.691(3)	1.686(8)	1.693(4)	1.537(3)
(*X*-O)	*1.661*	*1.646*	*1.684*	*1.690*	*1.709*	*1.538*
Reference	Our data	Kolitsch et al. 2004	Schmidt et al. 2005	Brahim et al. 2002	Rice and Robinson 1976	Ni et al. 1995

822

823

824

This is a preprint, the final version is subject to change, of the American Mineralogist (MSA)
Cite as Authors (Year) Title. American Mineralogist, in press.
DOI: https://doi.org/10.2138/am-2019-7028

825 Table 10. Parameters of Electron Backscatter Diffraction of gasparite-(La)
826 from the Ushkatyn-III deposit

Electron microscope model	Hitachi S-3400N
EBSD detector	Oxford HKL Nordlys Nano
Acceleration voltage, kV	30
Beam current, nA	0.3
Incidence angle, degrees	70
Sample Tilt	70
Exposure time, seconds per frame	5
Averaging, frames	20
ICSD number of reference structure	155917 (Schmidt et al. 2005)
Number of indexed bands	12 (max)
Mean angular deviation (MAD)	0.15

827

This is a preprint, the final version is subject to change, of the American Mineralogist (MSA)
Cite as Authors (Year) Title. American Mineralogist, in press.
DOI: https://doi.org/10.2138/am-2019-7028

Table 1. Chemical composition of gasparite-(La)

Constituent	Ushkatyn-III deposit		Wanni glacier	
	Wt%	**Range**	**Wt%**	**Range**
Fe_2O_3	0.05	0.00-0.16	0.00	0.00
MnO	1.30	0.91-1.96	0.00	0.00
CaO	1.33	0.97-1.54	0.34	0.24-0.48
ThO_2	0.00	0.00	0.58	0.37-0.72
Y_2O_3	0.01	0.00-0.05	0.01	0.00-0.03
La_2O_3	40.21	37.83-41.17	35.59	34.57-36.74
Ce_2O_3	10.69	9.76-11.61	22.55	21.26-23.67
Pr_2O_3	1.46	0.00-1.99	0.29	0.00-0.88
Nd_2O_3	4.24	3.53-4.69	1.04	0.50-1.30
Sm_2O_3	0.09	0.00-0.33	0.07	0.00-0.35
V_2O_5	9.77	8.58-11.21	0.00	0.00
P_2O_5	0.64	0.22-0.99	4.29	4.18-4.45
As_2O_5	30.32	29.46-31.41	34.48	33.27-35.22
Total	**100.11**		**100.13**	

This is a preprint, the final version is subject to change, of the American Mineralogist (MSA)
Cite as Authors (Year) Title. American Mineralogist, in press.
DOI: https://doi.org/10.2138/am-2019-7028

Table 2. Comparative crystallographic data for monazite group minerals

Mineral	Gasparite-(La)	Gasparite-(Ce)	Rooseveltite	Monazite-(La)	Monazite-(Ce)	Monazite-(Nd)	Monazite-(Sm)	Cheralite
Chemical formula	$La(AsO_4)$	$Ce(AsO_4)$	$Bi(AsO_4)$	$La(PO_4)$	$Ce(PO_4)$	$Nd(PO_4)$	$Sm(PO_4)$	$CaTh(PO_4)_2$
Crystal system	Monoclinic							
Space group	$P2_1/n$							
a (Å)	6.9576(4)	6.929(3)	6.879(1)	6.8313(10)	6.7880(10)	6.7352(10)	6.6818(12)	6.7085(8)
b (Å)	7.1668(4)	7.129(3)	7.159(1)	7.0705(9)	7.0163(9)	6.9500(9)	6.8877(9)	6.4152(6)
c (Å)	6.7155(4)	6.697(3)	6.732(1)	6.5034(9)	6.4650(7)	6.4049(8)	6.3653(9)	6.4152(6)
β (°)	104.414(1)	104.46(3)	104.84(1)	103.27(1)	103.43(1)	103.68(1)	103.86(1)	103.71(1)
Z	4							
Reference	Our data	Kolitsch et al. 2004	Bedlivy and Mereiter 1982	Ni et al. 1995				Raison et al. 2008

Note: for comparison u.c.p parameters given as *a*>*c*

This is a preprint, the final version is subject to change, of the American Mineralogist (MSA)
Cite as Authors (Year) Title. American Mineralogist, in press.
DOI: https://doi.org/10.2138/am-2019-7028

Table 3. Reflectance of gasparite-(La) from the Ushkatyn-III deposit measured in air

λ (nm)	**R_1**	**R_2**	**λ (nm)**	**R_1**	**R_2**
400	11.19	9.05	**560**	10.92	8.90
420	12.04	9.82	**580**	10.88	8.84
440	12.35	10.15	**589**	10.87	8.83
460	12.35	10.13	**600**	10.85	8.81
470	12.16	9.95	**620**	10.85	8.77
480	11.97	9.77	**640**	10.89	8.74
500	11.45	9.44	**650**	10.92	8.77
520	11.15	9.17	**660**	10.94	8.79
540	11.00	9.00	**680**	11.09	8.86
546	10.98	8.98	**700**	11.23	9.08

Table 4. Raman spectral signatures of gasparite-(La)

Raman shift (cm^{-1})	**Relative Intetsity (a.u.)**		**Assignment**	**Raman shift, (cm^{-1})**	**Relative Intetsity (a.u.)**		**Assignment**
	Ushkatyn-III	Wanni glacier			Ushkatyn-III	Wanni glacier	
92	0.6		Lattice vibrations	**364**	3		$v_4(AsO_4)$
94		*3*		**367**		*7*	$v_4(AsO_4)$
104	0.8			**379**	**73**		$v_2(AsO_4)$
107		*6*		**395**		*100*	$v_2(AsO_4)$
125		*6*		**421**		*28*	$v_4(AsO_4)$
126	0.3			**422**	9		$v_4(AsO_4)$
138	2			**452**	10		$v_4(AsO_4)$
139		*4*		**462**		*16*	$v_4(AsO_4)$
153	3			**812**		*4*	$v_3(AsO_4)$
155		*5*		**822**	**21**		$v_3(AsO_4)$
190	2	*7*		**826**		*9*	$v_3(AsO_4)$
203	**29**	*4*		**843**	8		$v_3(AsO_4)$
264	0.8			**848**		*74*	$v_3(AsO_4)$
267		*1*		**860**	**100**		$v_1(AsO_4)$
320	8			**864**		*86*	$v_1(AsO_4)$
334	4						
337		*12*					

This is a preprint, the final version is subject to change, of the American Mineralogist (MSA)
Cite as Authors (Year) Title. American Mineralogist, in press.
DOI: https://doi.org/10.2138/am-2019-7028

Table 5. Powder X-ray diffraction data for gasparite-(La) from Wanni glacier

I_{obs}	d_{obs}	I_{calc}	d_{calc}	*h*	*k*	*l*		I_{obs}	d_{obs}	I_{calc}	d_{calc}	*h*	*k*	*l*
9	5.39	5	5.39	1	0	-1		**19**	1.898	13	1.900	0	2	3
13	4.89	10	4.90	0	1	1		**6**	1.851	3	1.853	3	2	0
12	4.80	9	4.81	1	1	0		**19**	1.814	19	1.816	2	-2	-3
12	4.30	10	4.31	1	-1	-1				2	1.794	1	3	2
8	4.18	3	4.18	1	0	1				5	1.789	0	4	0
		5	3.61	1	1	1		**25**	1.780	22	1.780	2	3	1
20	3.574	16	3.577	0	2	0		**11**	1.727	10	1.728	0	4	1
64	3.361	58	3.363	0	0	2				3	1.681	0	0	4
6	3.249	5	3.249	2	0	0		**9**	1.673	8	1.673	2	0	-4
100	3.156	100	3.158	0	2	1				7	1.637	0	1	4
22	3.042	18	3.043	0	1	2		**17**	1.633	5	1.633	0	3	3
		26	2.968	2	-1	-1				2	1.633	4	-1	-1
77	2.956	69	2.958	2	1	0				2	1.631	4	0	-2
24	2.693	22	2.695	2	0	-2				5	1.624	4	0	0
19	2.519	18	2.524	2	-1	-2		**8**	1.619	3	1.618	2	1	3
19	2.511	12	2.506	2	1	1		**8**	1.587	6	1.590	4	-1	-2
8	2.446	5	2.450	0	2	2				2	1.584	4	1	0
6	2.407	6	2.410	2	-2	-1		**12**	1.579	5	1.579	2	-3	-3
5	2.301	3	2.304	1	0	-3				3	1.579	0	4	2
16	2.233	8	2.239	1	3	0		**7**	1.517	5	1.519	4	-2	-1
		8	2.230	3	0	-1				2	1.494	3	2	2
12	2.189	8	2.193	1	-1	-3		**6**	1.491	2	1.491	2	-4	-2
11	2.163	6	2.166	1	2	2		**4**	1.473	2	1.474	4	-1	-3
8	2.138	3	2.139	0	1	3		**6**	1.397	3	1.398	0	4	3
		2	2.021	2	-1	-3		**10**	1.379	8	1.380	4	2	1
33	2.004	31	2.006	2	1	2		**8**	1.374	6	1.372	4	-3	-1
9	1.941	4	1.942	1	-3	-2		**15**	1.362	3	1.364	2	-4	-3
30	1.923	28	1.925	2	-3	-1								

This is a preprint, the final version is subject to change, of the American Mineralogist (MSA)
Cite as Authors (Year) Title. American Mineralogist, in press.
DOI: https://doi.org/10.2138/am-2019-7028

Table 6. Crystal data, collection and structure refinement details for gasparite-(La) from Wanni glacier

Crystal Data	
Chemical formula	$(La_{0.60}Ce_{0.40})(As_{0.84}P_{0.16})O_4$
M_r	271.39
Crystal system, space group	Monoclinic, $P2_1/n$
a, b, c (Å)	6.7155 (4), 7.1668 (4), 6.9576 (4)
β (°)	104.414 (1)
V (Å^3)	324.32 (3)
Z	4
D_x (g/cm^3)	5.558
Crystal size (mm)	0.04 × 0.04 × 0.03
Data collection	
Diffractometer	Bruker *APEX*-II CCD
Radiation type	Mo$K\alpha$ (0.71073 Å)
μ (mm^{-1})	21.95
Absorption correction	Multi-scan
No. of measured, independent and observed [$I > 2s(I)$] reflections	3839, 944, 869
2Θ range for data collection (°)	7.55 to 60.00
Index ranges	$-9 \le h \le 9$, $-9 \le k \le 10$, $-9 \le l \le 9$
Refinement	
R_{int}, R_σ	0.0207, 0.0175
$R_1[F^2 > 2\sigma(F^2)]$, $wR_2(F^2)$, S	0.014, 0.029, 1.12
No. of reflections	944
No. of parameters	57
$\Delta\rho_{max}$, $\Delta\rho_{min}$ (e Å^{-3})	0.76, -0.55

Table 7. Fractional atomic coordinates and isotropic displacement parameters (U_{iso}, Å^2) for gasparite-(La) from Wanni glacier

Site	***x***	***y***	***z***	U_{iso}	**Occupancy (<1)**
M (4*e*)	0.40018 (2)	0.34494 (2)	0.21899 (2)	0.00827 (6)	$(La_{0.6}Ce_{0.4})$ *
X (4*e*)	0.38653 (4)	0.16300 (4)	0.69644 (4)	0.00626 (11)	$(As_{0.84}P_{0.16})$
O1 (4*e*)	0.2803 (3)	0.2142 (3)	0.8797 (3)	0.0131 (4)	
O2 (4*e*)	0.5664 (3)	-0.0012 (3)	0.7481 (3)	0.0133 (4)	
O3 (4*e*)	0.5031 (3)	0.3390 (3)	0.6113 (3)	0.0122 (4)	
O4 (4*e*)	0.1793 (3)	0.1075 (3)	0.5181 (3)	0.0130 (4)	

Note:* Occupancy of *M* site was fixed according to electron microprobe data.

This is a preprint, the final version is subject to change, of the American Mineralogist (MSA)
Cite as Authors (Year) Title. American Mineralogist, in press.
DOI: https://doi.org/10.2138/am-2019-7028

Table 8. Anisotropic displacement parameters (Å^2) for gasparite-(La) from Wanni glacier

Site	U^{11}	U^{22}	U^{33}	U^{12}	U^{13}	U^{23}
M	0.00902 (8)	0.00690 (9)	0.00836 (8)	0.00092 (6)	0.00117 (5)	0.00025 (6)
X	0.00599 (16)	0.00562 (17)	0.00700 (16)	-0.00001 (11)	0.00131 (11)	0.00013 (11)
O1	0.0119 (10)	0.0165 (11)	0.0105 (9)	-0.0006 (8)	0.0024 (8)	-0.0027 (8)
O2	0.0108 (10)	0.0086 (10)	0.0199 (10)	-0.0009 (8)	0.0029 (8)	-0.0012 (8)
O3	0.0162 (10)	0.0097 (10)	0.0117 (9)	-0.0033 (8)	0.0054 (8)	0.0009 (8)
O4	0.0119 (10)	0.0131 (11)	0.0120 (9)	0.0002 (8)	-0.0011 (8)	-0.0048 (8)

Table 9. Selected bond lengths (Å) and distortion of *M*-polyhedra
for gasparite-(La) from Wanni glacier
and structurally related *MX*O4 compounds (*M*=La, Ce; *X*=As, P, V).

Bond	**Length**					
	Gasparite-(La)	Gasparite-(Ce)	La(AsO_4)	Ce(AsO_4)	La(VO_4)	La(PO_4)
M—O1^{iii}	2.554 (2)	2.486(5)	2.571(3)	2.939(8)	2.521(4)	2.479(3)
M —O1^{iv}	2.481 (2)	2.527(5)	2.489(3)	2.636(9)	2.497(3)	2.554(3)
M —O2^{v}	2.479 (2)	2.902(5)	2.498(4)	2.460(7)	2.656(3)	2.783(3)
M —O2^{ii}	2.559 (2)	2.544(4)	2.560(4)	2.619(8)	2.568(3)	2.589(3)
M —O3^{ii}	2.901 (2)	2.632(5)	2.655(3)	2.472(8)	2.528(4)	2.615(3)
M —O3^{vi}	2.562 (2)	2.620(6)	2.577(3)	2.551(7)	2.677(4)	2.503(3)
M —O3	2.6440 (19)	2.457(5)	2.912(4)	2.562(7)	2.887(4)	2.672(3)
M —O4^{iii}	2.624 (2)	2.488(5)	2.644(4)	2.476(7)	2.533(4)	2.466(3)
M —O4^{vii}	2.472 (2)	2.555(4)	2.486(3)	2.543(7)	2.502(4)	2.548(3)
(*M*-O)	*2.586*	*2.579*	*2.599*	*2.584*	*2.597*	*2.579*
Δ*M*	*0.035*	*0.036*	*0.035*	*0.038*	*0.037*	*0.030*
X—O1	1.650 (2)	1.647(5)	1.670(4)	1.682(8)	1.724(4)	1.523(3)
X—O2	1.660 (2)	1.664(5)	1.680(4)	1.699(7)	1.720(4)	1.553(3)
X—O3	1.669 (2)	1.659(5)	1.695(4)	1.692(7)	1.699(4)	1.541(3)
X—O4	1.6656 (19)	1.615(5)	1.691(3)	1.686(8)	1.693(4)	1.537(3)
(*X*-O)	*1.661*	*1.646*	*1.684*	*1.690*	*1.709*	*1.538*
Reference	Our data	Kolitsch et al. 2004	Schmidt et al. 2005	Brahim et al. 2002	Rice and Robinson, 1976	Ni et al. 1995

Table 10. Parameters of Electron Backscatter Diffraction of gasparite-(La)
from the Ushkatyn-III deposit

Electron microscope model	Hitachi S-3400N
EBSD detector	Oxford HKL Nordlys Nano
Acceleration voltage, kV	20
Beam current, nA	1
Incidence angle, degrees	70
Sample Tilt	0
Exposure time, seconds per frame	0.5
Averaging, frames	20
ICSD number of reference structure	155917 (Schmidt et al. 2005)
Number of indexed bands	12 (max)
Mean angular deviation (MAD)	0.1053

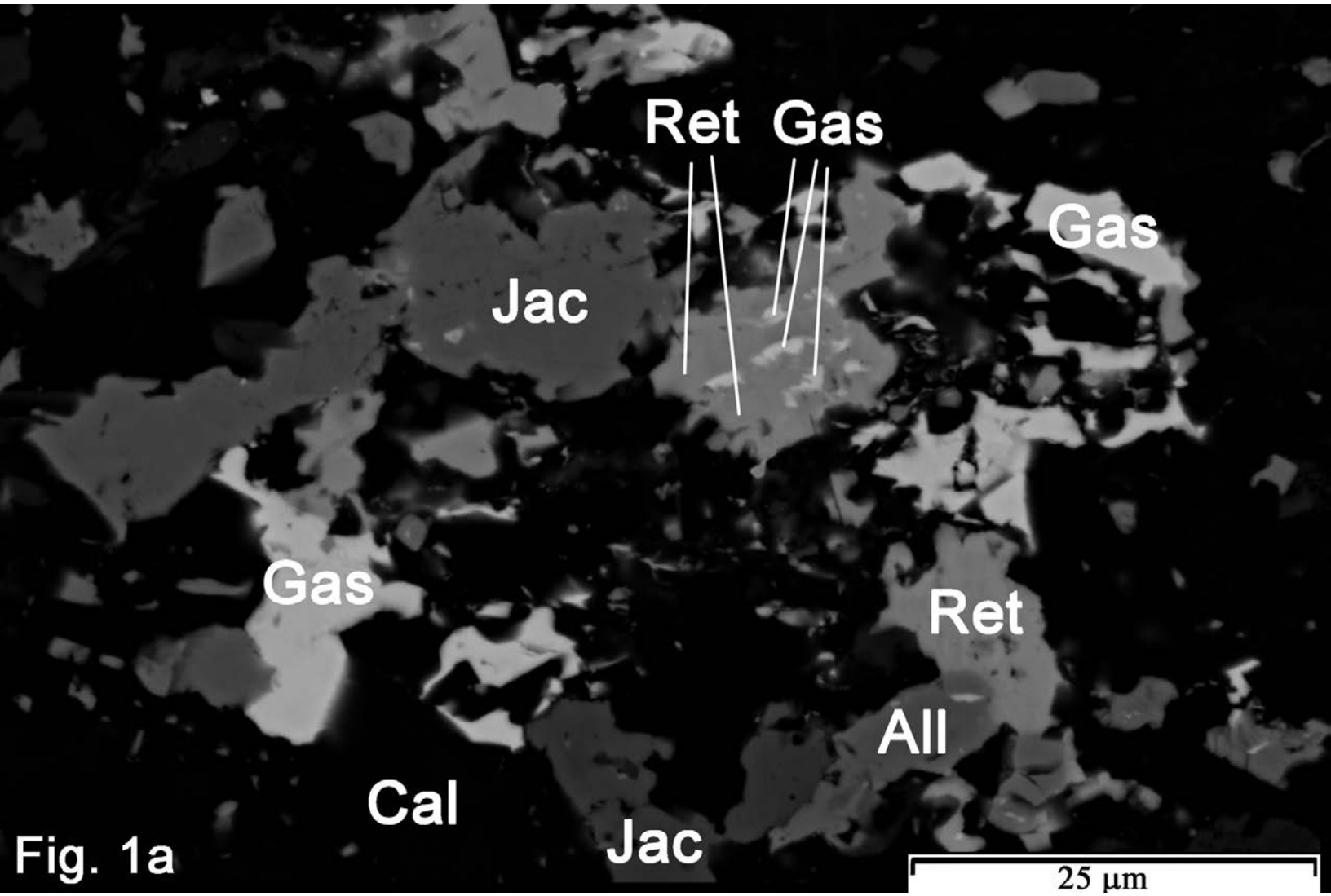

Fig. 1a

Fig. 1b

Fig.2

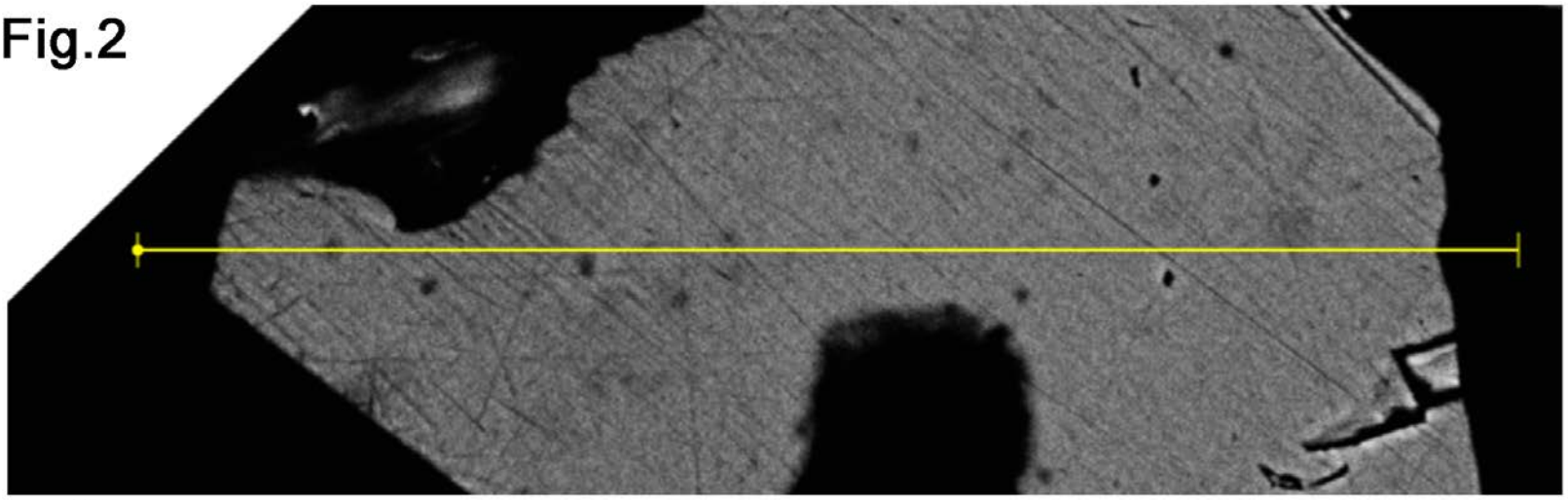

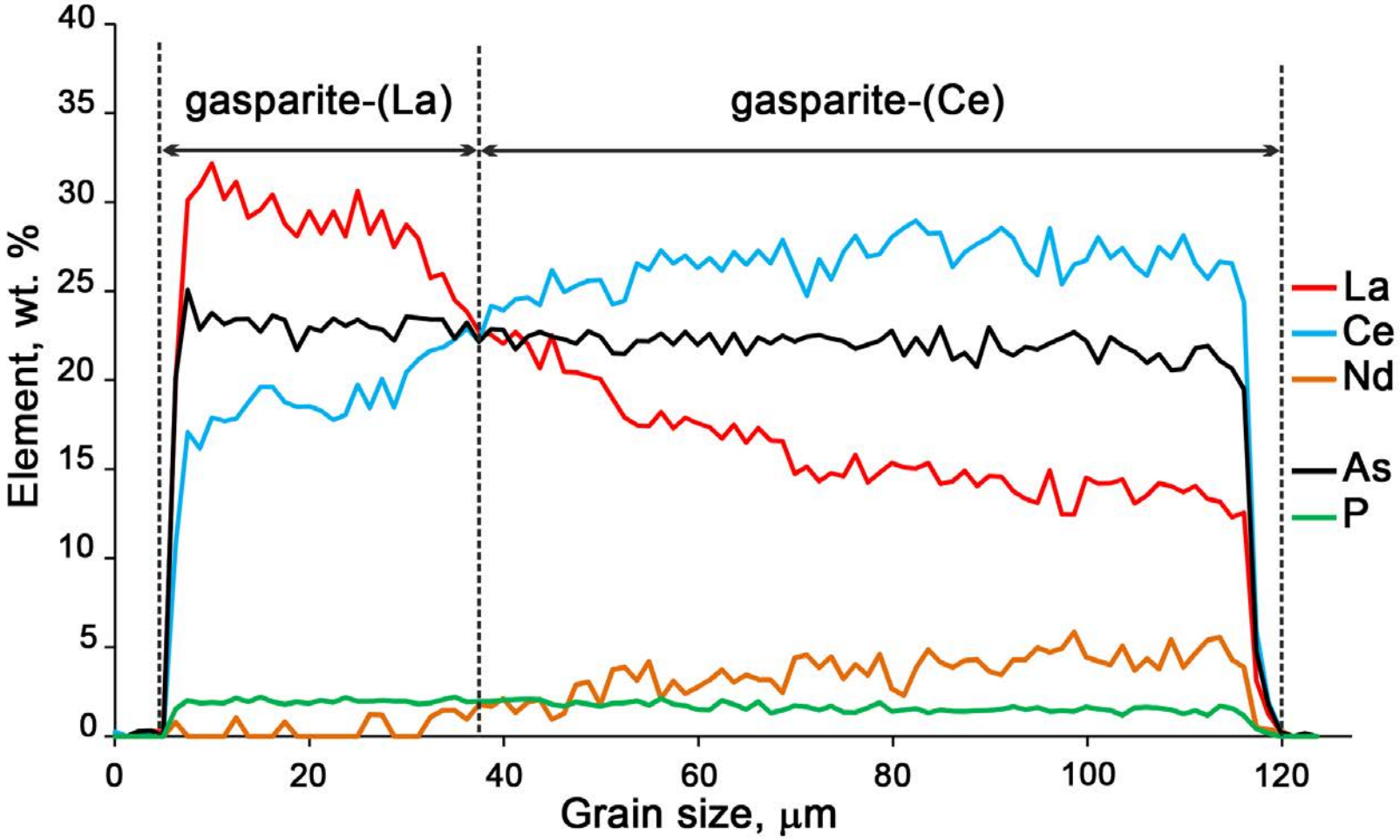
gasparite-(La)
gasparite-(Ce)
Element, wt. %
Grain size, μm
0
5
10
15
20
25
30
35
40
0
20
40
60
80
100
120
La
Ce
Nd
As
P

Fig. 3

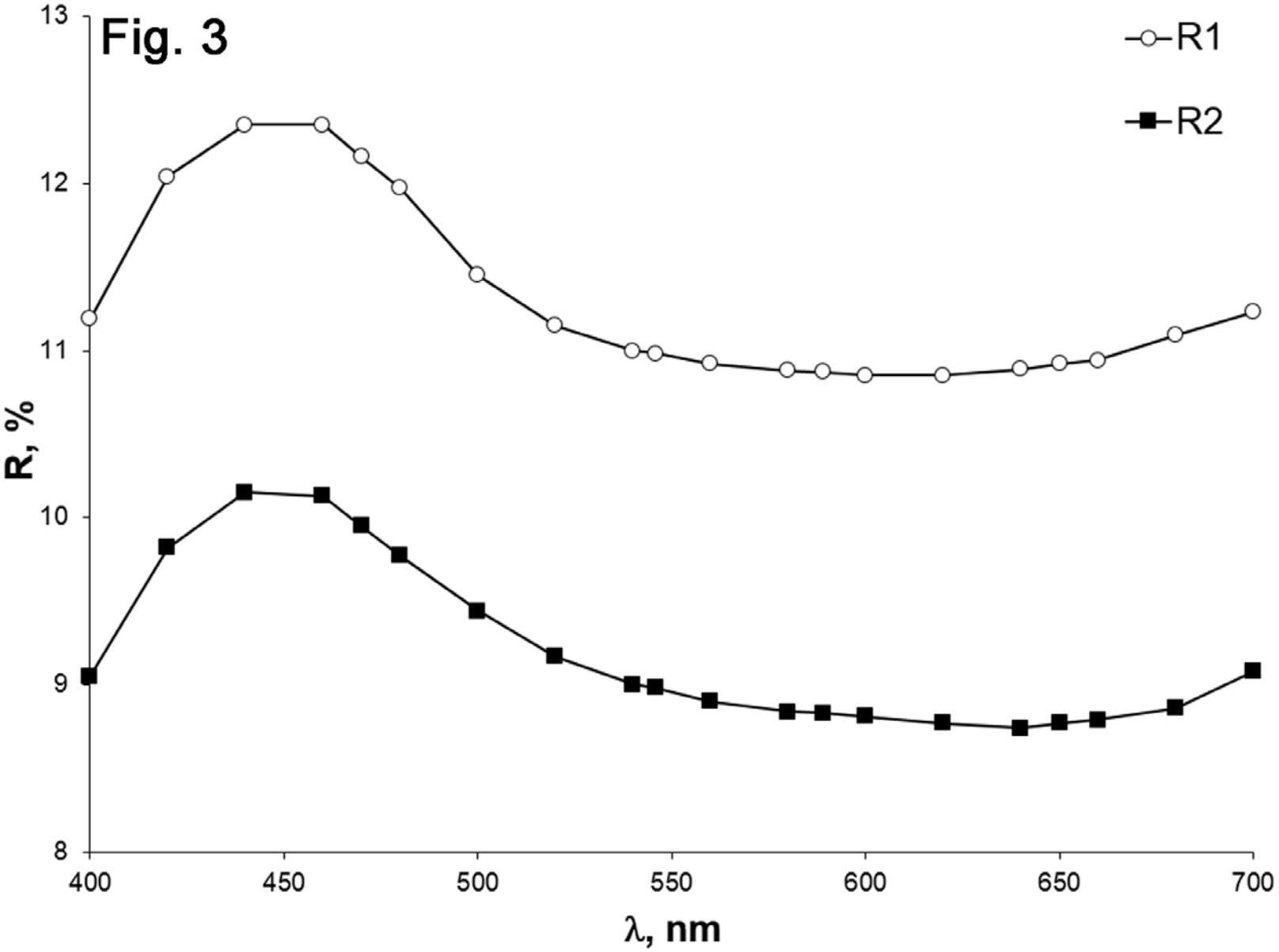

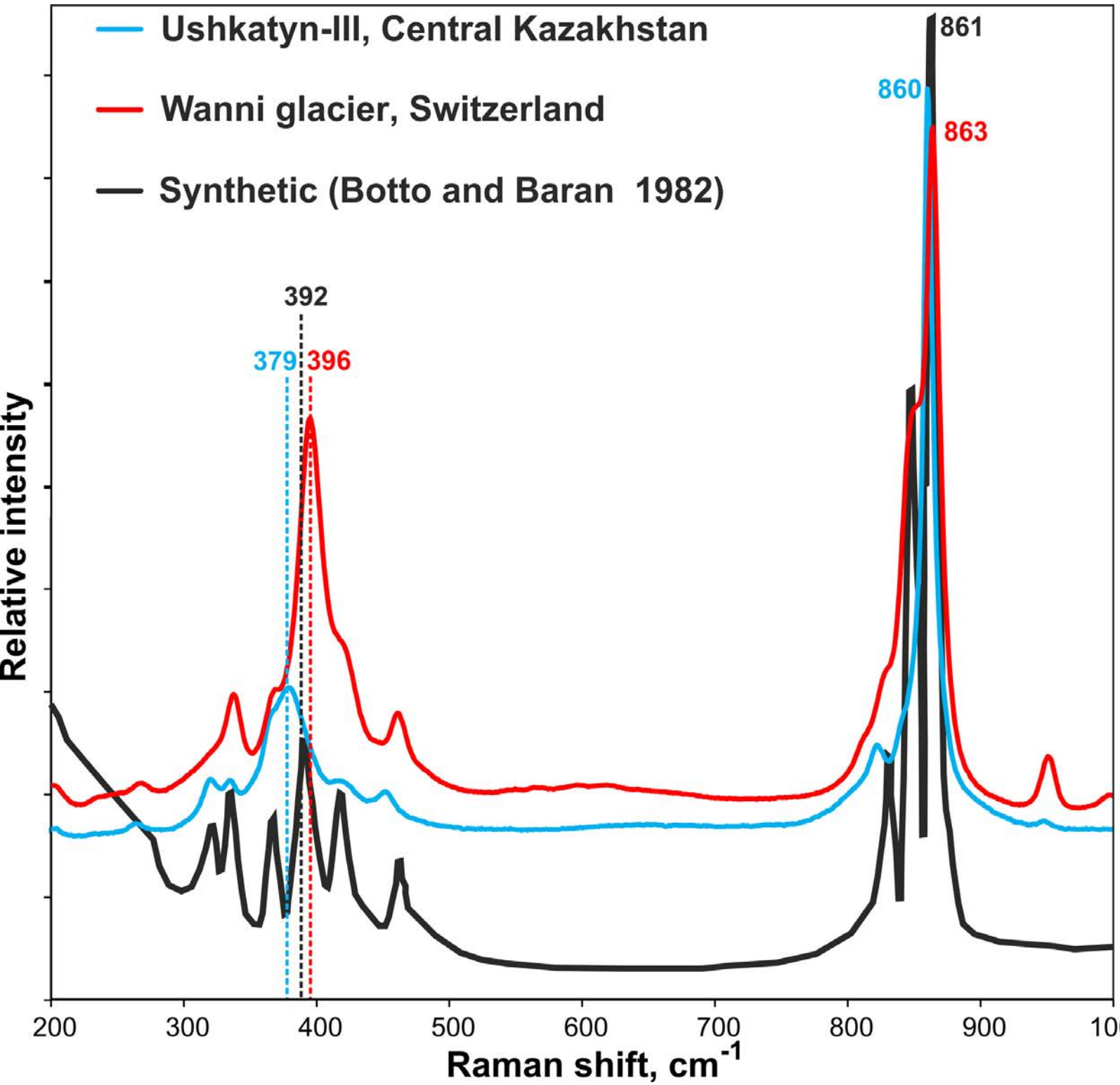
Ushkatyn-III, Central Kazakhstan
Wanni glacier, Switzerland
Synthetic (Botto and Baran 1982)
861
860
863
392
379
396
Relative intensity
200
300
400
500
600
700
800
900
1000
Raman shift, cm-1

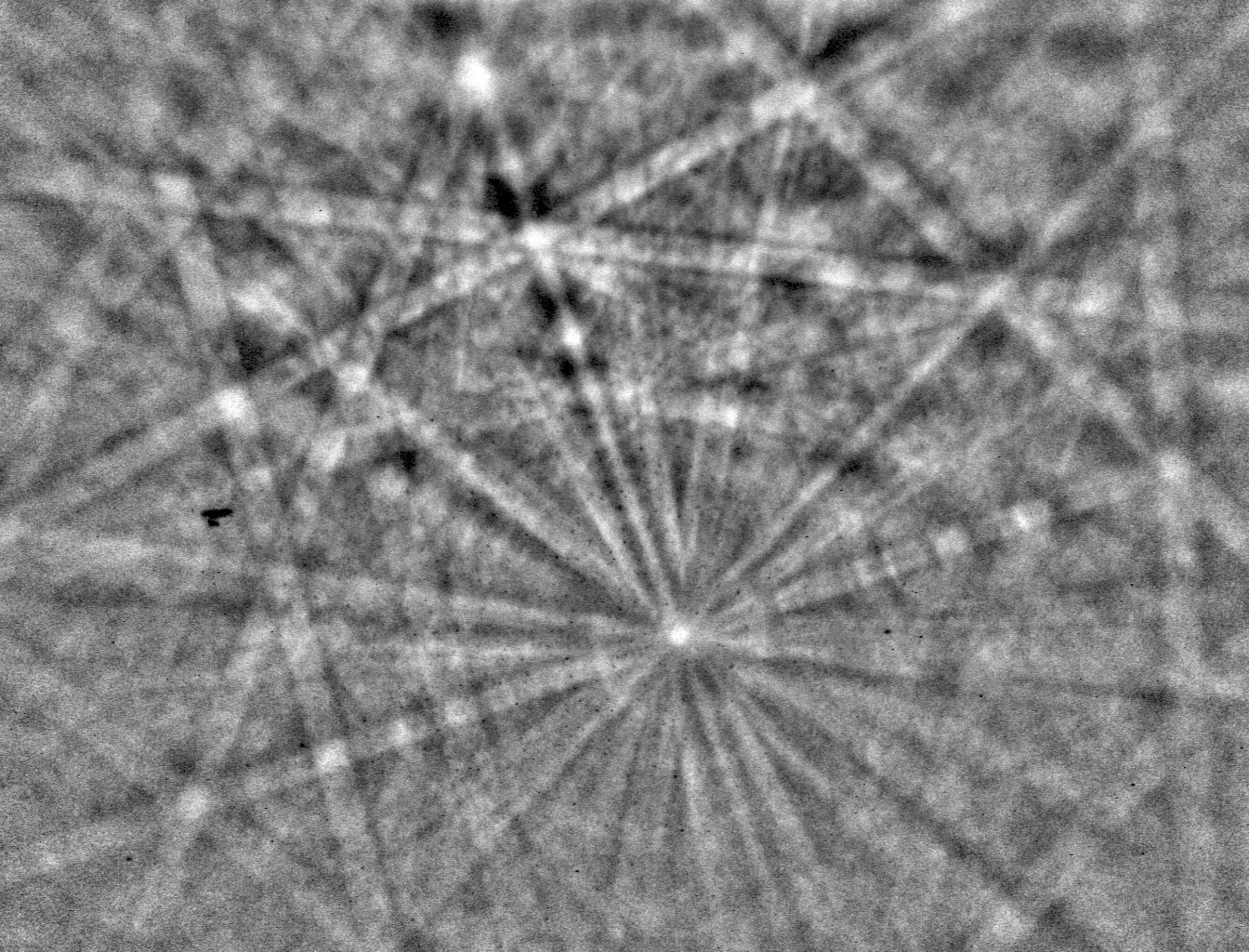

Fig. 6a

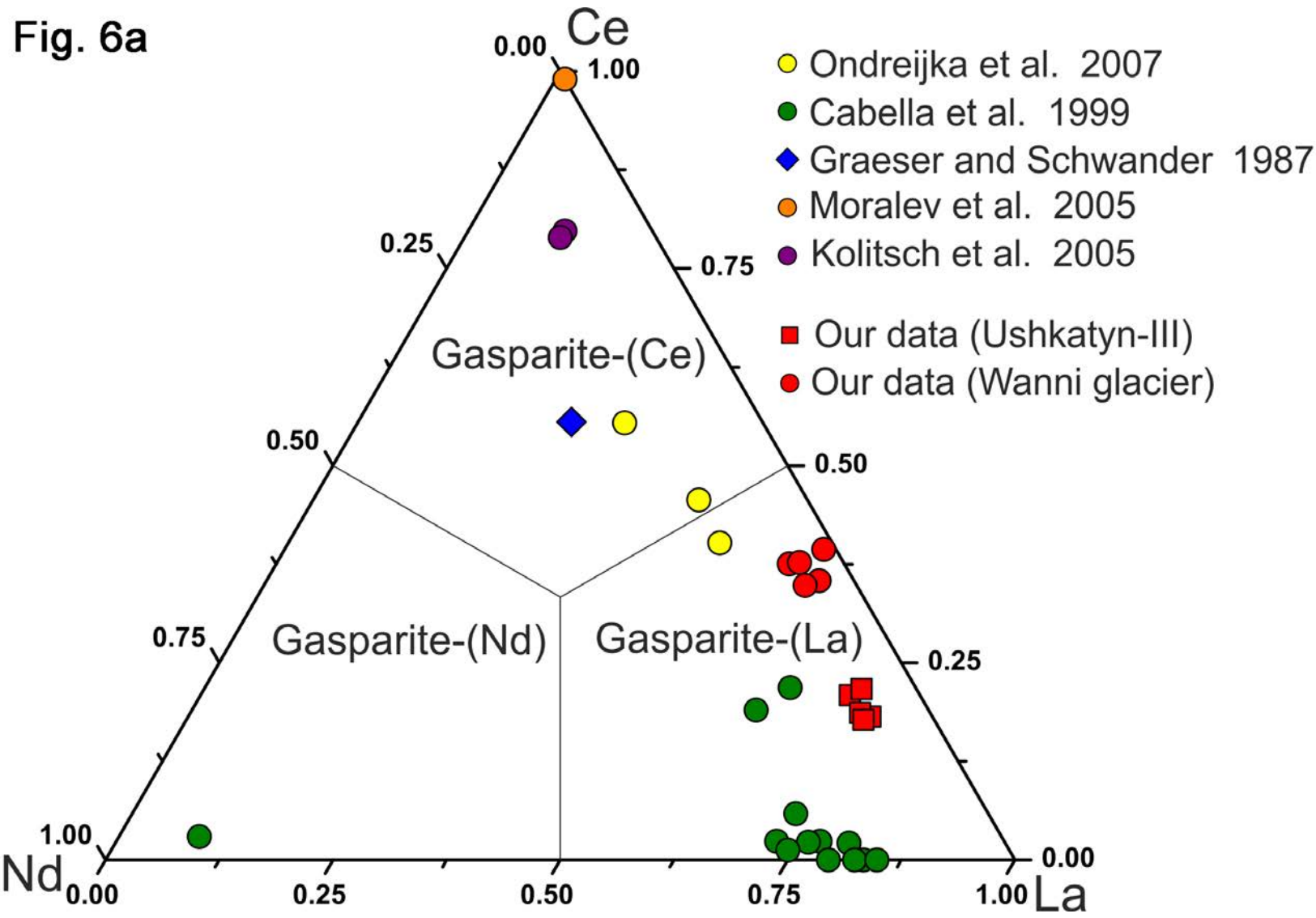
Ce
0.00
1.00
0.25
0.75
0.50
0.50
0.75
0.25
1.00
0.00
Nd
0.00
0.25
0.50
0.75
1.00
La
Gasparite-(Ce)
Gasparite-(Nd)
Gasparite-(La)
Ondreijka et al. 2007
Cabella et al. 1999
Graeser and Schwander 1987
Moralev et al. 2005
Kolitsch et al. 2005
Our data (Ushkatyn-III)
Our data (Wanni glacier)

Fig. 6b

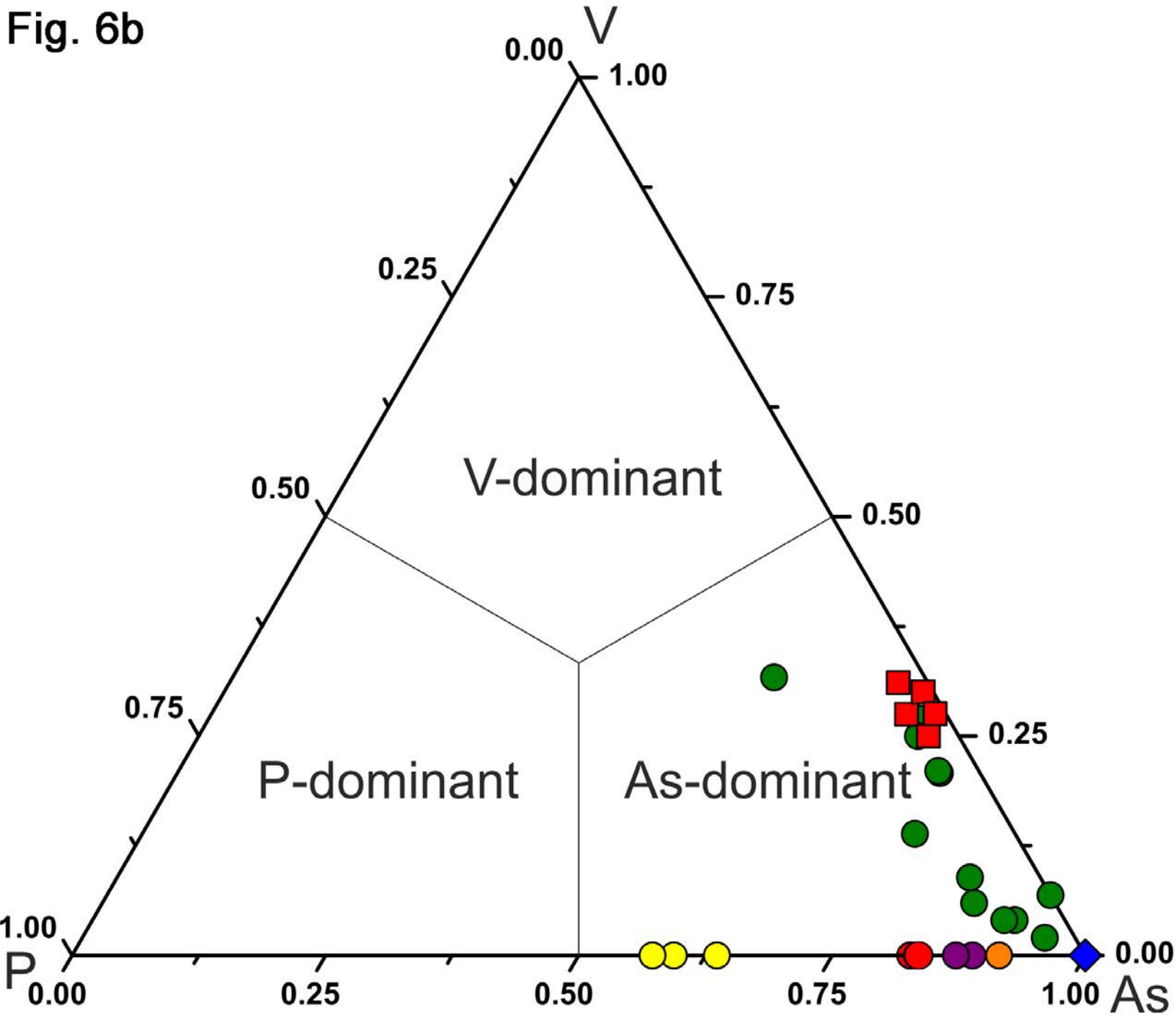
V
0.00
1.00
0.25
0.75
0.50
0.50
0.75
0.25
V-dominant
P-dominant
As-dominant
1.00
P
0.00
0.00
0.25
0.50
0.75
1.00
As

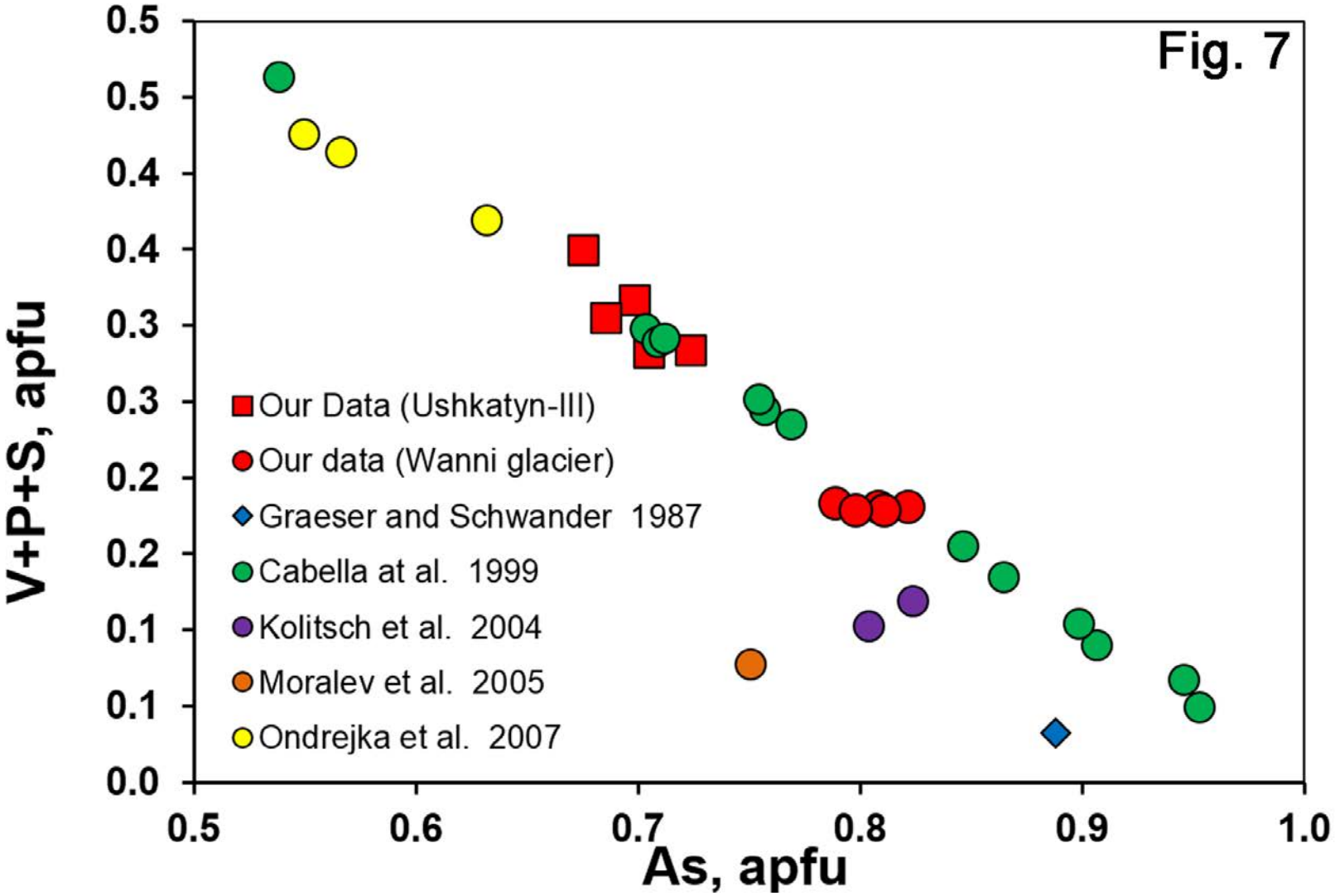
Fig. 7
V+P+S, apfu
As, apfu
0.0
0.1
0.1
0.2
0.2
0.3
0.3
0.4
0.4
0.5
0.5
0.5
0.6
0.7
0.8
0.9
1.0
Our Data (Ushkatyn-III)
Our data (Wanni glacier)
Graeser and Schwander 1987
Cabella at al. 1999
Kolitsch et al. 2004
Moralev et al. 2005
Ondrejka et al. 2007

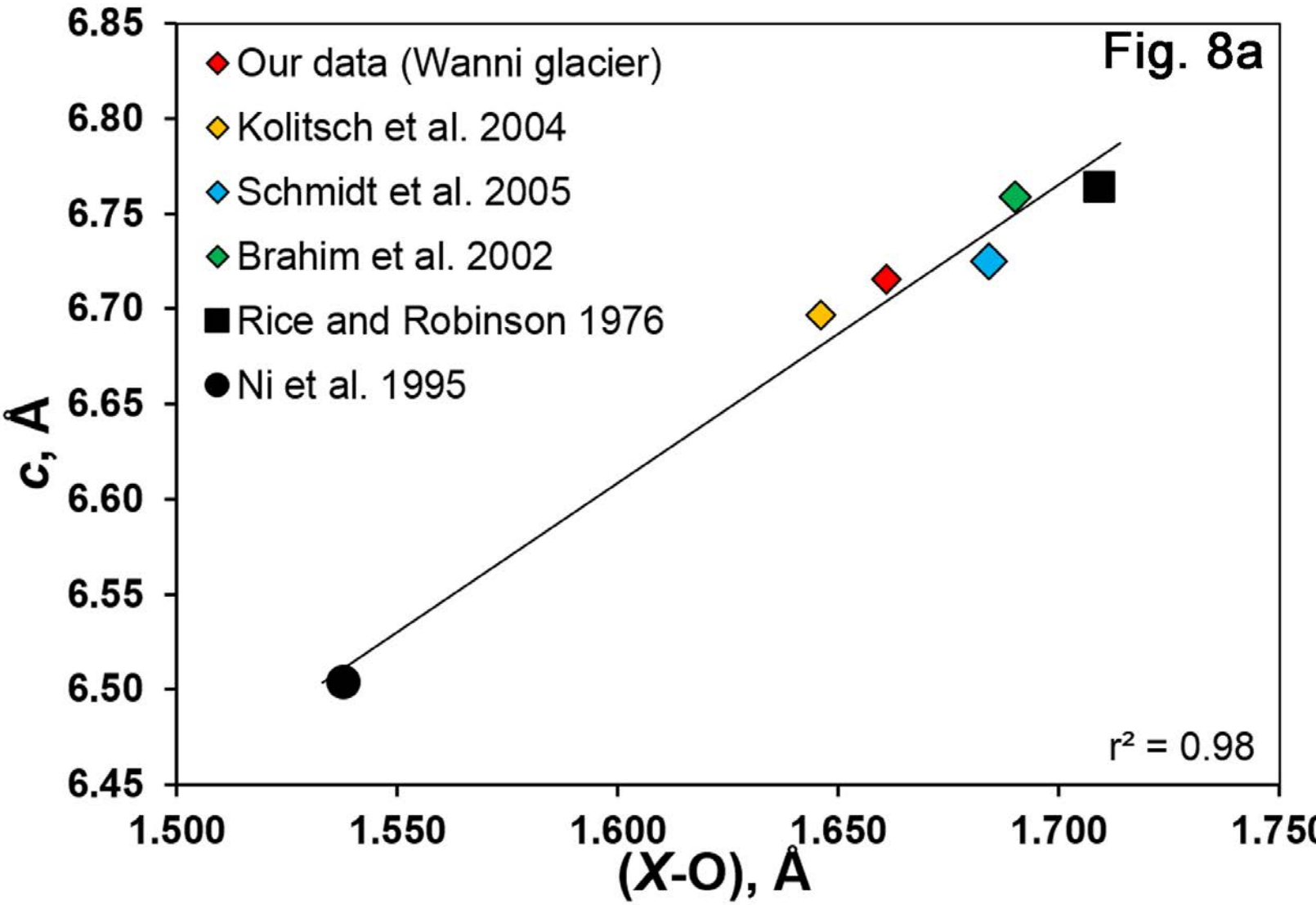
Fig. 8a
Our data (Wanni glacier)
Kolitsch et al. 2004
Schmidt et al. 2005
Brahim et al. 2002
Rice and Robinson 1976
Ni et al. 1995
r² = 0.98
c, Å
(X-O), Å
6.85
6.80
6.75
6.70
6.65
6.60
6.55
6.50
6.45
1.500
1.550
1.600
1.650
1.700
1.750

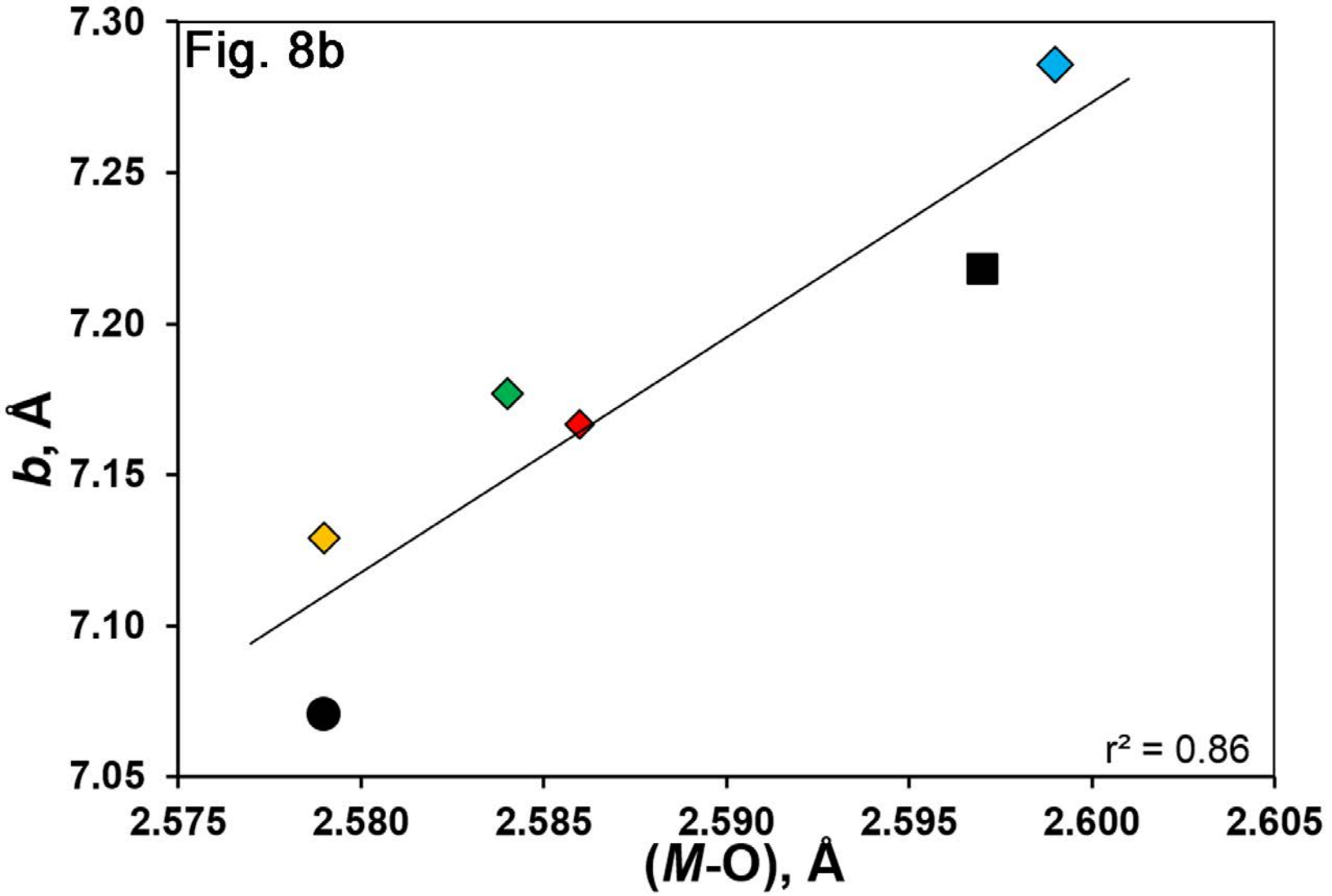
Fig. 8b
7.30
7.25
7.20
7.15
7.10
7.05
b, Å
2.575
2.580
2.585
2.590
2.595
2.600
2.605
(M-O), Å
r² = 0.86

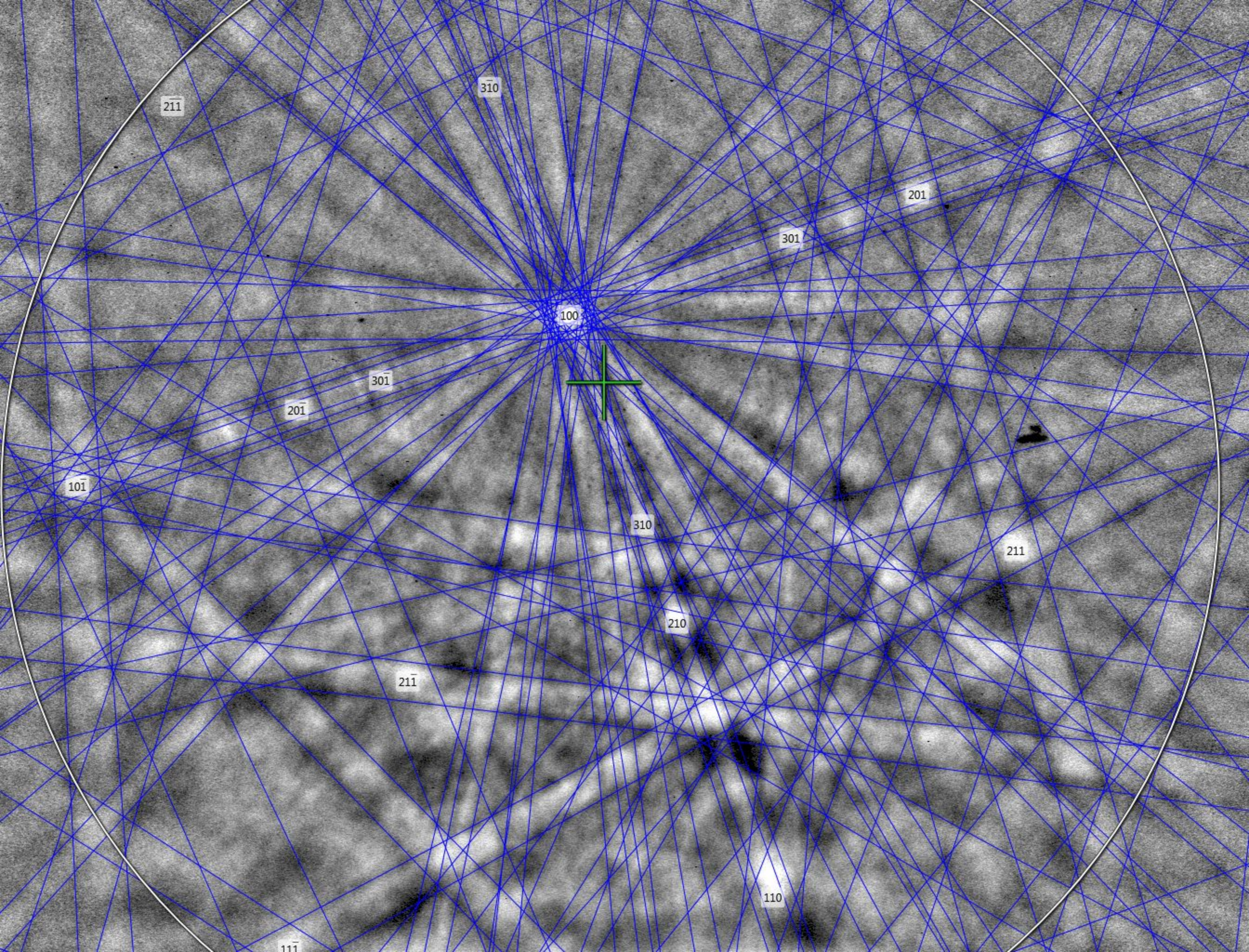
$2\bar{1}\bar{1}$
$3\bar{1}0$
201
301
100
$30\bar{1}$
$20\bar{1}$
$10\bar{1}$
310
211
210
$21\bar{1}$
110
$11\bar{1}$